

Organic and Hybrid Solar Cells Based on Small Molecules

Luiz C. P. Almeida, Jilian N. de Freitas, Flavio S. Freitas
and Ana F. Nogueira

Abstract In this chapter, the recent literature involving small molecule-based organic solar cells (OSCs) will be reviewed. The number of papers published in the fields of organic semiconductor and OSCs has grown exponentially in the past decade. Such growth is stimulated by the exciting properties of these materials, combined with the possibility to produce colored, flexible, transparent and cheap solar cells. The main focus of this review is to give an overview and a perspective of the recent advances in this area, highlighting the most interesting results, novel materials as well as their limitations and challenges. This chapter will explore the properties and applications of several classes of small organic molecules, as electron donors and acceptors, dyes, and hole transport materials. Different architectures and techniques will be also discussed in the assembly of double, heterojunction, and multilayer films.

1 Introduction

“Size is not important”. This well-known adage is heard everywhere when the matter is size (and in most cases, in a positive perspective). In the field of organic semiconductors (OSs) and in particular those involving organic field-effect transistors, organic light-emitting devices and organic solar cells (OSCs), size has been demonstrated to be an irrelevant factor. Indeed, the best performing devices are those based on a limited number of low-molecular weight materials.

L. C. P. Almeida · J. N. de Freitas · F. S. Freitas · A. F. Nogueira (✉)
Chemistry Institute, University of Campinas-UNICAMP,
P.O. Box 6154, Campinas, SP 13083-970, Brazil
e-mail: anaflavia@iqm.unicamp.br

There are currently two major classes of OSs: the low-molecular weight materials, or small molecules, and π -conjugated polymers such as poly(thiophenes), poly(fluorine), and poly(phenylene vinylenes) derivatives. They have many features in common, such as their excitonic nature (excitons are electrically neutral quasi-particles consisting of bound electron-hole pairs formed after photoexcitation), low dielectric constants, localized charge carriers (electrons and holes), optically and electrically anisotropic properties, high extinction coefficients, narrow absorption bands, and more disordered structures compared to inorganic semiconductors.

Organic semiconductors, both small molecules and polymers, show great promise for photoconversion through their synthetic variability, low-temperature processing (similar to that applied to plastics), and the possibility of producing lightweight, flexible, easily manufactured, and inexpensive solar cells.

Although OSCs have been known for more than 50 years, they have become the subject of active research only in the past 20 years. This new generation of solar cells is also referred to as nanostructured solar cells since at least one component and/or the morphology is in the nanoscale range. Low-temperature processing of organic small molecules and polymers from the vapor-phase or from solution have a crucial advantage over silicon technology since the high-temperature processing requirements of the latter increases the production cost and limits the range of substrates on which they can be deposited. Additionally, OSs can be easily applied using low-cost methods, such as the high-speed, roll-to-roll technique. Unfortunately, despite significant advances, the power-conversion efficiency of OSCs remains low, with maximum values in the range of 6–7%. When at least one component is replaced by an inorganic counterpart, these solar cells are referred to as hybrid devices. Dye-sensitized solar cells (DSSC) fit well in this class. For this kind of solar cell, the efficiency is $\sim 11\%$, but has remained at this plateau in the last years.

In order to enhance their competitiveness with other technologies, efficiency and long-term stability are crucial in the field of OSC. The photocurrent in these solar cells is limited by the light-harvesting capability of the individual molecules or polymers in the device. Small band gap molecules have been intensively studied to overcome these drawbacks, but it is a complicated matter. Morphology is also important in this context because it impacts charge transport and an intimate contact between donor and acceptor materials in a nanoscale range is difficult to achieve due to phase separation. A better understanding of these processes at the material level, particularly those in layer-to-layer interfaces, which determine the open-circuit voltage (V_{OC}), is critical and remains the subject of active research. For DSSCs, photoelectrochemical devices, an additional factor is the presence of a liquid electrolyte, which can hamper large-area production.

In this chapter, the application of small organic molecules applied to organic or hybrid solar cells (including DSSCs) will be reviewed. A detailed description of the chemical, physical, and electrical properties of OSs, or the state of art of OSCs based on π -conjugated polymers is not the focus of this chapter. For this purpose, the reader is encouraged to see references [1–7].

Although many small molecules have been known and studied for decades, only a small fraction have been used successfully in OSCs. This reflects the diversity in charge-carrier mobilities, exciton diffusion lengths, thin film morphology, energy levels, band gap, absorption coefficient and ambient and thermal stability. In this chapter, we present the most commonly used donor and acceptor materials used as active layers in OSCs and the most important contributions in this field will be highlighted.

This chapter will be divided into five sections. The first two deal with small molecules applied to OSCs, separated by fabrication techniques: physical and solution methods. The third and fourth sections deal with liquid crystals (LCs) and three-component solar cells, respectively, using diverse techniques. The last section involves a description of small molecules in dye-sensitized solar cells as sensitizer and hole transport materials.

2 Solution-Processable OSC

Solution-processable OSCs (SPOSC), prepared using solution processing techniques including spin-coating, casting, roll-to-roll, etc., have attracted increasing attention in academia and industry because of their potential advantages. Such advantages include easy fabrication, low-cost, low-weight, large-area production, and mechanical flexibility. On the other hand, films formed from blend solutions tend to phase separate. The scale of the phase separation depends on the solvent, solubility of the materials and other parameters associated with deposition, such as the speed and temperature of the spin-coating process. The nanomorphology of the active layer film is very important to device efficiency. Also, the materials used in solution-processed solar cells must fulfill the physical conditions of high charge-carrier mobilities, suitable values of highest occupied molecular orbital (HOMO) and lowest unoccupied molecular orbital (LUMO) energy levels, strong absorption in the visible region and several processing conditions, such as: (i) the materials must be soluble in common organic solvents, (ii) the solubility has to be high enough to enable the deposition of smooth thin films, or even thick films, (iii) the morphology of the spin-casted films should have the desired structure concerning phase separation on the exciton diffusion length-scale and the percolation path to the electrodes.

In this section, we present a review of recent reports on the use of small molecule-based OSC assembled using solution-processing methods. This kind of solar cell is analogous to the bulk-heterojunction devices based on polymer and fullerenes, which are not in the scope of this review. Concerning the efficiencies, OSCs based on small processable molecules are considered to be less efficient, but, recent reports have demonstrated the potential of the small molecules and efficiencies are catching up to those of the “standard” bulk-heterojunction devices.

The first achievement in the area of SPOSC was to make the small molecules soluble in organic solvents. Before their use in organic or hybrid solar cells, most

small molecules must undergo several chemical modifications in order to be made appropriate for a solution-deposition method. Even the buckminsterfullerene, C₆₀, had to be converted into its well-known soluble derivative, [6, 6]-phenyl-C₆₁-butyric acid methyl ester (PCBM). Most of the significant achievements have been realized with chemically modified molecules.

For example, perylene and its derivatives have been combined with different molecules and polymers in SPOSCs. Li et al. [8] investigated a blend of perylene tetracarboxydiimide as the acceptor and the polymer poly[*N*-(20-decyltetradecyl)carbazole]-2,7-diyl as the donor. The bulk-heterojunction device based on this combination afforded 0.63% of overall power-conversion efficiency (η) under low light intensity illumination (10 mW cm⁻²). Sharma et al. [9] reported the fabrication of photovoltaic devices using a bulk-heterojunction layer of a small molecule named compound T (Fig. 1a), containing a central *p*-phenylenevinylene unit, an intermediate thiophene moiety, and terminal 4-nitrophenyl-cyano-vinylene as the donor, and a perylene-pyrene bisimide (Fig. 1b) as the acceptor. At the optimum blend ratio (donor:acceptor 1:3.5 wt%), η was \sim 1.9%. The efficiency was further increased to \sim 3.2% when the device was annealed (100°C for 5 min) and a thin ZnO layer was incorporated between the active layer and the Al electrode.

Squaraine dyes are another class of molecules which have been the subject of many recent investigations, owing to their unique photochemical/photophysical properties. The attraction to these dyes includes their broad absorption spectrum (550–900 nm), facile synthetic access, a wide variety of possible structures and oxygen/moisture stability. These properties enable an active layer deposition under ambient conditions, in contrast to the inert atmosphere required for most conducting polymers. New soluble squaraine derivatives (Fig. 1c) were used as long-wavelength absorbers and donor components in SPOSC, and the effects of core modification on active layer film morphology and photovoltaic response were investigated [10]. Both linear and branched alkyl chain substituents provide solubility, but each gave rise to different effects on the solid state organization [11]. SPOSCs with different squaraine:PCBM ratios were fabricated by spin-coating the blends from chloroform or *o*-dichlorobenzene. The optimum annealing conditions were found to be 70°C for 1 h, as evidenced by the increased phase separation observed in atomic force microscopy (AFM) images. Devices fabricated with a 1:3 squaraine:PCBM ratio spin-cast from chloroform exhibited higher carrier mobility and improved performance, with a short-circuit current (J_{SC}) of 5.70 mA cm⁻² and an efficiency of 1.24%. This value was 1.5 times higher than the result obtained using *o*-dichlorobenzene and was attributed to microstructure evolution effects that occur during a more rapid film growth and drying rate when using chloroform [10].

Recently, Winzenberg et al. [12] reported the polycyclic aromatic template dibenzo[*b,def*]chrysene as a promising candidate for use in organic electronic devices. These compounds have an advantage over other well-studied small molecules, such as pentacenes, because they do not undergo cycloaddition reactions with fullerenes. The bulk-heterojunction solar cells made from a

dibenzo[*b,def*]chrysene compound (Fig. 1d) and PCBM reached an efficiency of 2.25%. These findings encouraged the use of other unexplored polycyclic aromatic compounds in solution-processable bulk-heterojunction solar cells.

Other molecules, such as, anthradithiophene [13], merocyanine [14], or dendritic thiophene [15] derivatives, shown in Fig. 1e–g, have been used in solution processed, small molecule-based devices in the last few years. Amine-based molecules were also explored as possible candidates for highly efficient SPOSCs. Two isomeric compounds (Fig. 1h–i) containing a dibenzo[*f,h*]thieno[3,4-*b*]quinoxaline core and two peripheral arylamines were synthesized. The bulk-heterojunction SPOSC based on these materials as sensitizers and PCBM as electron acceptor exhibited efficiency of 1.70%, which was attributed to the balanced electron and hole mobility found in the active layer film [16].

Triphenylamine (TPA) molecules are also potential candidates for OSCs. These molecules possess 3D, propeller-like geometry, glass-forming properties, and a relatively high oxidation potential. TPA derivatives have shown excellent thermal and electrochemical stability, electron-donating ability, isotropic optical, and charge-transport properties [17, 18]. Research efforts have led to a progress in the synthesis of new molecules which mainly consist of a TPA moiety linked to different acceptor moieties, including dicyanovinyl, perylene, benzothiadiazole (BT), or 2-pyran-4-ylidenemalononitrile, aiming at the development of donor- π -acceptor (D- π -A) structures. Molecules with D- π -A structure have many advantages, such as a lower bandgap which arises from the intramolecular charge transfer between the donor and acceptor, and easily controlled energy levels by introducing acceptor and donor moieties with different pull–push electron abilities into the molecules [19, 20]. Compared with the D- π -A type polymers, soluble D- π -A small molecules have the advantages of well-defined molecular structure, monodispersity, and relatively simple and reproducible synthesis and purification, making them promising materials for application in solution-processing solar cells.

New solution-processable molecules, shown in Fig. 2, based on the combination of TPA donor units and BT acceptor units have been synthesized recently [21–24]. He et al. [21] compared the properties of devices based on the star-shaped molecule S(TPA-BT) and the linear molecule L(TPA-BT) (see Fig. 2). The S(TPA-BT) film showed a broader and stronger absorption band in the range of 440–670 nm, lower band gap, higher hole mobility and better film-forming properties (high quality uniform spin-cast film) than those of the corresponding linear L(TPA-BT). The devices assembled with PCBM as acceptor and S(TPA-BT) reached a J_{SC} of 4.2 mA cm⁻², V_{OC} of 0.81 V, FF of 0.39 and 1.3% of efficiency, while those based on L(TPA-BT) showed J_{SC} of 1.25 mA cm⁻², V_{OC} of 0.84 V, FF of 0.34 and 0.35% of efficiency. The same group later investigated a molecule with TPA as core and benzothiadiazole-(4-hexyl) thiophene as arms, S(TPA-BT-4HT). The end group of 4-hexylthiophene in S(TPA-BT-4HT) instead of the TPA end group in S(TPA-BT) was intended to further improve the film morphology and photovoltaic properties. The SPOSC devices were fabricated by spin-coating the blended solution of S(TPA-BT-4HT) and [6, 6]-phenyl-C₇₁-butyric acid methyl ester (PC₇₁BM) (1:3, w/w) and by using a Mg/Al electrode.

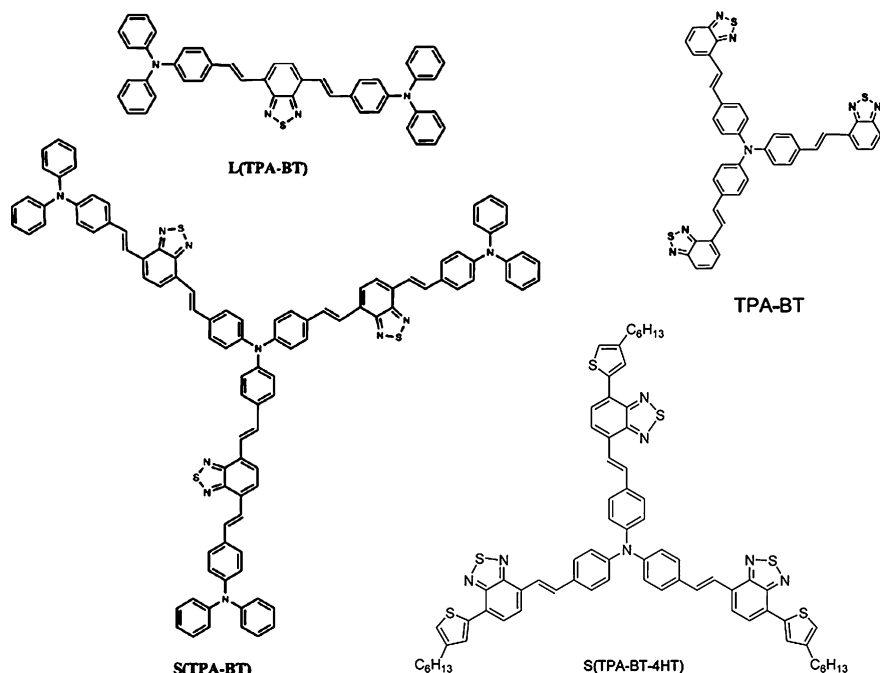


Fig. 2 Examples of linear and star-shaped molecules consisting of a TPA moiety linked to different acceptor moieties [21, 22]

The obtained J_{SC} was 8.58 mA cm^{-2} , V_{OC} of 0.85 V and FF of 32.7%, resulting in maximum efficiency of 2.4% [22].

D- π -A structures containing electron-accepting sulfonyldibenzene cores and electron-donating TPA dendrons have also been synthesized. Since the dendrimers were highly soluble in common organic solvents, they were used to assemble bulk-heterojunction SPOSCs in combination with PCBM, by spin-coating [25]. The cell based on dendrimer G0 (Fig. 3) showed an efficiency of only 0.34%. This might be related to the absorption characteristics of the molecule, which strongly absorbs light only below 450 nm. Devices fabricated with other molecules with similar structures (G1 and G2, Fig. 3) had even lower performances. Although the larger molecules G1 and G2 absorb photons at longer-wavelengths when compared to G0, their extinction coefficients are lower than that of G0.

2-[2,6-bis-[2-(4-styryl)-vinyl]-pyran-4-ylidene]malononitrile (DCM)-type organic dyes have also been combined with TPA. DCM dyes are known as low-molecular weight red-emitting materials and most of them have a D- π -A molecular structure that contains (dicyanomethylene)pyran (PM) as the electron acceptor. The strong electron-withdrawing PM group can lower the LUMO energy level and extend the absorption band such that it nearly overlaps with the entire visible spectrum when combined with strong electron-donating units. Moreover, the strong intermolecular dipole-dipole interaction or intermolecular π -stacking of

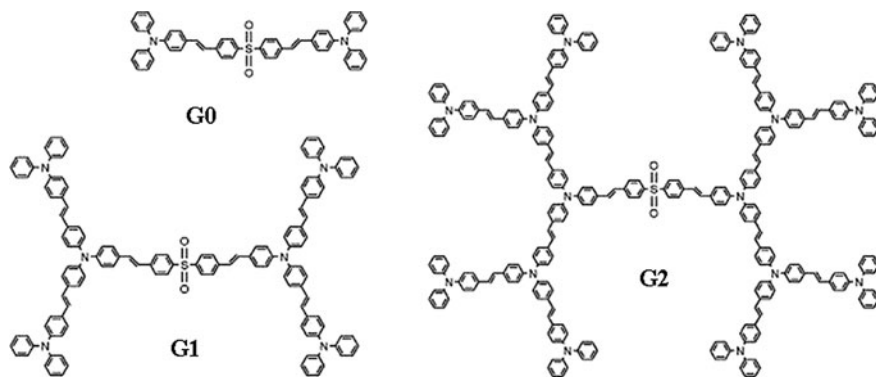


Fig. 3 Chemical structures of D- π -A molecules containing sulfonyldibenzene cores and TPA dendrons [25]

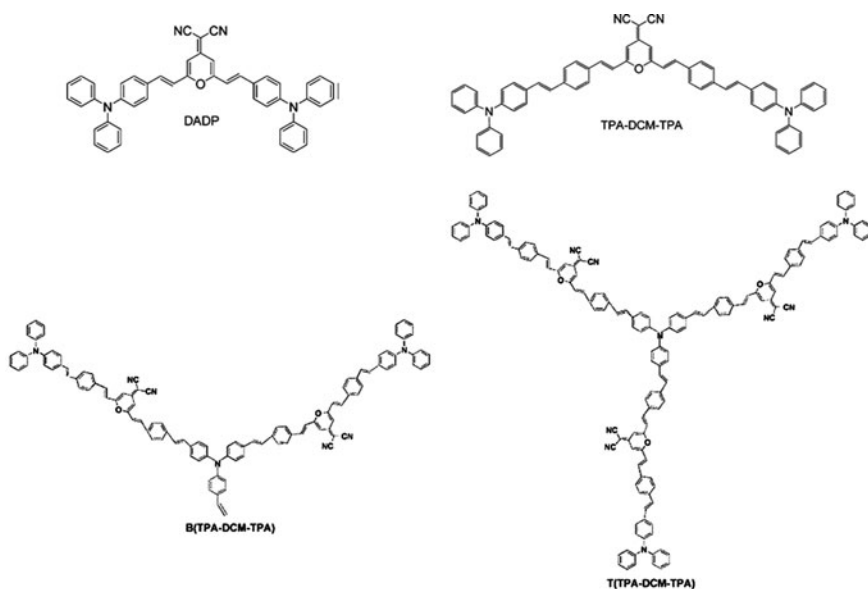


Fig. 4 Examples of D- π -A small molecules used in SPOSC, containing TPA groups linked to PM groups [26–28]

DCM-type organic dyes may be beneficial to the charge-carrier transportation. The combination of electron-rich TPA and electron deficient PM groups via π -conjugated spacers is also an interesting combination, since they can effectively reduce the band gap and produce special physical and photoelectric properties.

He et al. [26] reported the synthesis of a symmetric D- π -A small molecule TPA-DCM-TPA where two TPA groups are linked by divinylbenzene bridges at both ends of the PM group (Fig. 4). This material was applied in SPOSC and gave an efficiency of 0.79%.

Another symmetrical dye molecule, DADP (Fig. 4), was also used in a SPOSC [27]. The optimized bulk-heterojunction devices based on the combination of this dye and PCBM as the acceptor exhibited a J_{SC} of 4.16 mA cm^{-2} , V_{OC} of 0.98 V, FF of 0.37, and efficiency of 1.50%. The efficiency of the device based on DADP was almost twice that of the device based on TPA-DCM-TPA, although there is only a small difference between their molecular structures: DADP has a shorter distance between the TPA group and the PM group than TPADCM-TPA. This small structural difference results in a lower-lying HOMO energy level and a higher hole mobility in DADP, leading to increased efficiency.

Zhao et al. [28] synthesized bi-armed B(TPA-DCM-TPA) and tri-armed T(TPA-DCM-TPA) molecules, shown in Fig. 4. Although the B(TPA-DCM-TPA) and T(TPA-DCM-TPA) films show broad and strong absorption band in a wavelength range of 300–750 nm, when B(TPA-DCM-TPA) was used as the electron donor in an OSC with PCBM as the electron acceptor, the devices delivered a power-conversion efficiency of only 0.73%.

Phthalocyanines (PC) and porphyrins (PP) have also been successfully used in SPOSCs. In fact, the first efficient OSC based on small molecules reported by Tang [29] had PC as the donor material. Several examples of binary blends involving PP have also been reported, designed for narrow-band absorption at the end of the visible spectrum [30, 31]. However, higher efficiencies were found for copper phthalocyanine/ C_{60} p-n junction devices [32], due to the longer exciton diffusion length in PC films as compared to PP films, which is reported to be as high as 68 nm [33].

The solution processing of the small molecule subnaphthalocyanine (SubNc) was developed by Ma et al. [34]. Due to the high solubility, low tendency to aggregate and strong light absorption in the visible region, amorphous SubNc films with high charge transporting and light-harvesting properties were prepared via solution casting. By using SubNc as the donor and C_{60} as the acceptor in a planar heterojunction SPOSC, the authors reported a power-conversion efficiency of 1.5%, with a V_{OC} of 0.55 V, J_{SC} of 5.6 mA cm^{-2} , and FF of 0.49. This device performance was considered high for a planar heterojunction device based on solution processable small molecules, and was assigned to the contribution of triplet excitons from SubNc.

Soluble 1,4:8,11:15,18:22,25-tetraethano-29*H*,31*H*-tetrabenzob[*b,g,l,q*]porphyrin (CP), which can be thermally converted to a highly insoluble and crystalline tetrabenzoporphyrin (BP) donor (Fig. 5), was used with a new fullerene acceptor bis(dimethylphenylsilylmethyl) C_{60} (SIMEF, Fig. 5) in a three-layered p-*i*-n structure, in which the *i*-layer possessed a defined interdigitated structure, formed by spontaneous crystalline phase separation during thermal processing [35]. This device showed a power-conversion efficiency of 5.2%, a value that is among the best reported for solution-processed small-molecule OSCs.

Huang et al. [36] synthesized two soluble alternating porphyrin-dithienothiophene conjugated copolymers where the units are linked by a single bond (I) or triple bond (II), as shown in Fig. 6. The absorption spectrum of a thin film of I exhibited a sharp Soret band at 450 nm and two weak Q-bands at 563–619 nm,

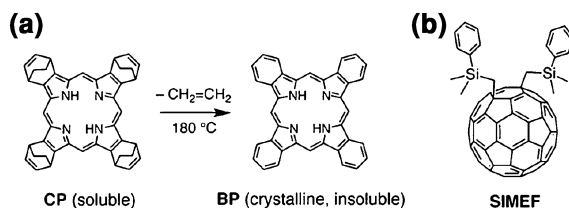


Fig. 5 Donor and acceptor materials used in SPOSC: **a** thermal retro-Diels–Alder conversion of CP (donor precursor) to BP (donor) at 180°C; **b** SIMEF (acceptor). “Reprinted with permission from Matsuo et al. [35]. Copyright 2009 American Chemical Society”

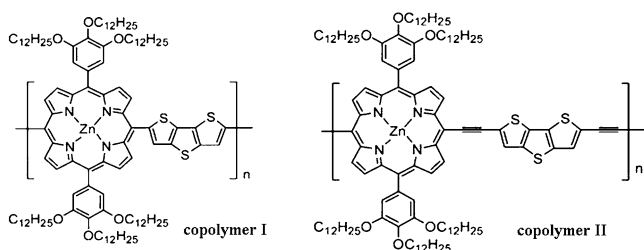


Fig. 6 Chemical structures of porphyrin-dithienothiophene copolymers containing single (I) or triple bonds (II) [36]

while II exhibited a sharp Soret band at 491 nm and a strong Q-band at 760 nm. The field-effect hole mobilities were measured to be $2.1 \times 10^{-4} \text{ cm}^2 \text{ V}^{-1} \text{ s}^{-1}$ for the two copolymers. Solar cells based on blends of these copolymers with PCBM were prepared by spin-coating an *o*-dichlorobenzene solution, followed by drying at 80°C for 30 min. Despite the high charge-carrier mobilities, the efficiencies obtained were only 0.30 and 0.15% for devices using II:PCBM or I:PCBM as active layer. Although the authors do not comment on the low efficiency values obtained, they attribute the difference observed to the stronger Q-band absorption shown by the copolymer II.

Recently, efficiencies of 2.3 and 3.0% were reported for devices combining the electron-poor diketopyrrolopyrrole-containing low-dimensional oligothiophene 2,5-di-(2-ethylhexyl)-3,6-bis-(500-*n*-hexyl)-[2, 20, 50, 200]terthiophen-5-yl-pyrrolo [3,4-*c*]pyrrole-1, 4-dione (SMDPPEH, Fig. 7) as donor, with PCBM or PC₇₁BM as acceptors [37–39]. Aiming at further exploring film morphology formation and its effects on device performance as a function of donor–acceptor (DA) interactions, Tamayo et al. [40] fabricated solar cells using SMDPPEH and methanofullerene derivatives having alkyl substituents with different lengths (as shown in Fig. 7). The authors observed that the absorption, crystallinity, film morphology, and device performance characteristics of both as-cast and annealed blended films of diketopyrrolopyrrole-based donors and fullerene acceptors are significantly affected by the length of the alkyl substituent attached to the methanofullerene. The domain size of these structures increased when the alkyl chain attached to the

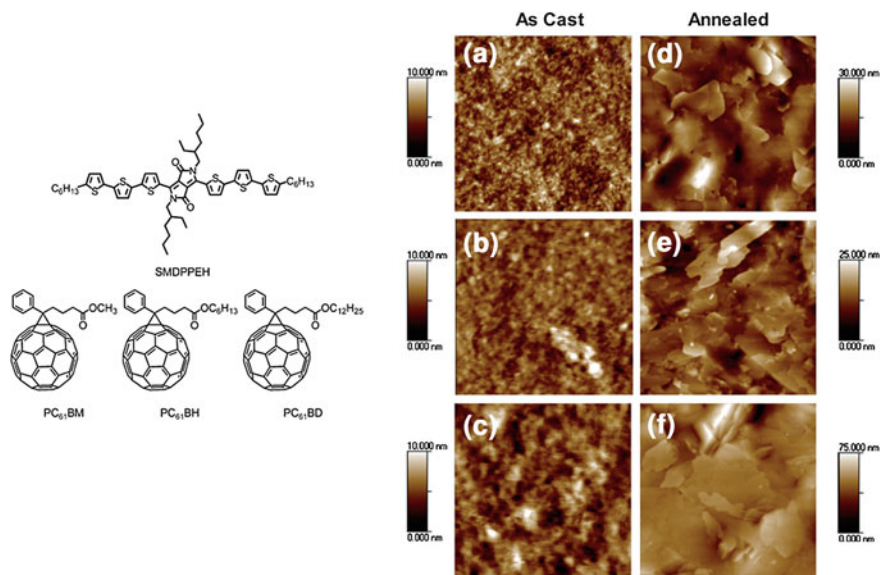


Fig. 7 Chemical structures of the donor SMDPPEH and the methanofullerene derivatives acceptors PC₆₁BM, PC₆₁BH and PC₆₁BD, which contain alkyl substituents with different lengths. AFM topographic images of as-cast (a, b, c) and annealed (d, e, f) SMDPPEH:PC61BX (50:50) from (2% w/v) solution where X = M = methyl (a and d), X = H = *n*-hexyl (b and e), X = D = *n*-dodecyl (c and f). Images for the as-cast and annealed films are 1 $\mu\text{m} \times 1 \mu\text{m}$ and 2 $\mu\text{m} \times 2 \mu\text{m}$ in size, respectively. Ref. [40]—reproduced by permission of The Royal Society of Chemistry (<http://dx.doi.org/10.1039/B912824G>)

fullerene acceptor was increased. Furthermore, annealing the blended films led to varying degrees of phase separation and the most pronounced phase separation was observed for the fullerene containing the largest alkyl chain. The different morphologies observed are shown in Fig. 7, and are believed to have resulted from the differences in hydrophobicity of the methanofullerenes, which affects their interaction with the relatively more polar donor material. Thus, the simple variation of the alkyl chain length results in devices with power-conversion efficiencies between 1.5 and 3%.

To date, OSCs exhibiting fill factor (FF) values exceeding 50% have only been realized with fullerenes [41–43], TiO₂ [44], or CdSe [45] as electron acceptors. However, the V_{OC} of these devices seldom exceeds 0.7 V, which is in part due to the high electron affinity of the electron-accepting phase, while an V_{OC} exceeding 1 V would be desirable for high power generation. On the other hand, V_{OC} values reaching 1.5 V have been obtained when blending suitable electron-donating and accepting polymers [46–48], but the FF of these devices was below 40% in most cases.

In this context, 2-vinyl-4,5-dicyanoimidazole (Vinazene) has been used as a precursor to design a novel family of electron-accepting materials in which, by changing the central aromatic unit, the energy of the LUMO can be tuned to sufficiently low values. Ooi et al. [49] employed the small-molecule

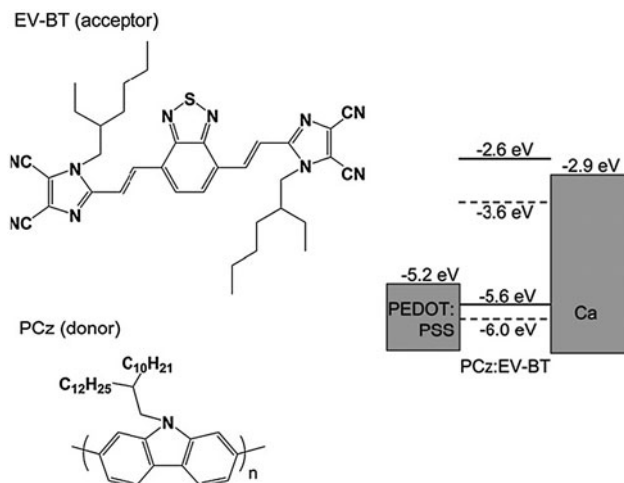


Fig. 8 Chemical structure of the donor polymer PCz and the acceptor molecule EV-BT. The *dashed lines* indicate the HOMO and LUMO levels of EV-BT and the *solid lines* those of PCz. Ooi et al. [49]—reproduced by permission of The Royal Society of Chemistry (<http://dx.doi.org/10.1039/B813786M>)

electron-acceptor EV-BT (Fig. 8) based on Vinazene in a SPOSC. This material has a LUMO level of 3.6 eV and strongly absorbs light in the visible region up to 520 nm. These properties make this material attractive when compared to the most widely used acceptor, PCBM. This Vinazene derivative was incorporated into bulk-heterojunction devices using a poly(2,7-carbazole) (PCz) as electron donor. This material provided absorption in a complementary range region and its HOMO level was found to be 5.6 eV. The devices were fabricated by spin-coating PCz:EV-BT films from chloroform solutions and the influence of blend composition and annealing temperature were investigated using different weight ratios of PCz:EV-BT. The most efficient device was obtained using 70% EV-BT followed by annealing at 80°C, which presented a high V_{OC} of 1.36 V and FF of 49%, but a low J_{SC} of 1.14 mA cm⁻², yielding an efficiency of only 0.75%.

Schubert et al. [50] investigated devices comprised of another Vinazene acceptor, 4,7-bis[2-(1-hexyl-4,5-dicyano-imidazol-2-yl)vinyl] benzo[c][1, 2, 5]-thiadiazole, (HV-BT, in Fig. 9), and poly(2,5-dimethoxy-1,4-phenylenevinylene-2-methoxy-5-(2-ethylhexyloxy)1,4-phenylenevinylene) (MEH-PPV) as the electron donor. Since HV-BT is soluble in common organic solvents, it can also be deposited by thermal evaporation; the authors were able to vary the device preparation scheme, systematically varying the heterojunction topology. Figure 9 shows the scheme of these devices, AFM images of the topology, current–voltage curve (J–V) and incident photon to current efficiency (IPCE) curves. The as-prepared bulk-heterojunction blend provided relatively low FF and IPCE values of 0.26 and 4.5%, respectively, attributed to significant recombination of geminate pairs and free carriers in a highly intermixed blend morphology. In the all-solution processed bilayer device, the FF

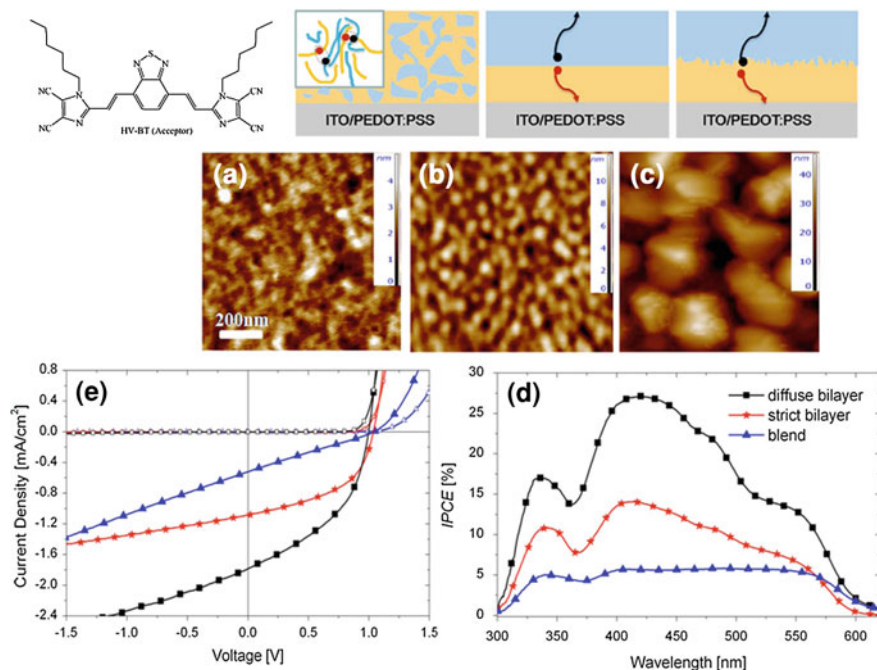


Fig. 9 Chemical structure of HV-BT and schematic depicting the interface topology at the donor/acceptor heterojunction for a blend device (*left*), the discrete bilayer with a vacuum processed acceptor layer deposited on top of the solution-cast polymer film (*center*), and the all-solution-processed bilayer device (*right*). A closed view of geminate pair recombination is shown in the *inset* of the left drawing. AFM topography images of **a** as-prepared 1:1 MEH-PPV:HV-BT blend spin-coated from chlorobenzene, **b** high-vacuum deposited HV-BT film on top of a MEH-PPV interlayer, and **c** pure HV-BT film spin-coated on top of the MEH-PPV interlayer. The **d** IPCE and **e** J–V curves measured under 100 mW cm⁻², AM 1.5 illumination, of an as-prepared 1:1 MEHPPV: HV-BT blend (*blue triangles*), a strict bilayer (*red stars*) with an evaporated HV-BT layer, and a diffuse bilayer (*black squares*) solar cell with solution-processed HV-BT on top of a MEH-PPV interlayer. “Reprinted with permission from Schubert et al. [50]. Copyright (2009), American Institute of Physics”

and IPCE dramatically increased to 0.43 and 27%, respectively. The FF increases further to 0.57 in devices comprised of thermally deposited Vinazene layers when there is virtually no interpenetration at the donor/acceptor interface. The AFM images in Fig. 9 suggests that both the solution-cast and evaporated HV-BT layers consist of crystallites. Such nanocrystalline morphology allows for the photogenerated electrons to quickly migrate into the acceptor phase away from the hetero-interface, thereby reducing the mutual Coulomb binding energy to the hole remaining in the donor phase. A high V_{OC} of about 1.0 V was nearly the same for all devices. This suggests that the heterojunction topology does not affect the energetics of the active layer or at the electrodes.

In a more recent work, Inal et al. [51] reported the photovoltaic properties of HV-BT combined with poly(3-hexylthiophene) (P3HT) (Fig. 10). The P3HT/

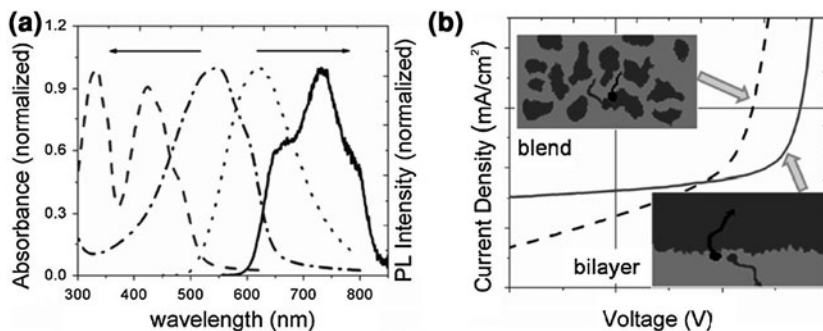


Fig. 10 **a** Normalized absorbance and photoluminescence spectra of thin films of P3HT (*dash-dotted* and *solid line*, respectively) and of HV-BT (*dashed* and *dotted line*, respectively). PL spectra were recorded at the excitation wavelengths of absorption maxima of each material. **b** J–V characteristics for bulk-heterojunction (*solid line*) or bilayer-type (*dashed line*) devices prepared with HV-BT and P3HT. Inal et al. [51]. Copyright Wiley–VCH Verlag GmbH & Co. KGaA. Reproduced with permission

HV-BT blend covers a broader spectral range (from 290 to 820 nm) than the HV-BT/MEH-PPV system. The photoluminescence (PL) intensity from the individual components was largely reduced in the blend and calculations showed that at least 95% of the excited states on both the donor and the acceptor are quenched in the non-annealed blend. The solar cells were fabricated with as-prepared 1:1 donor/acceptor mixtures and exhibited higher FF and IPCE when compared to earlier studies on blends of HV-BT with polymers [50, 52, 53]. This was attributed to the high molecular weight of the polymer sample used, which might assist the rapid motion of holes moving away from the heterojunction, rendering the photovoltaic properties less sensitive to the nanomorphology of the blend. No improvements were observed upon annealing the samples. On the other hand, a significant improvement of FF and V_{OC} was observed when inducing phase separation at a longer length-scale, i.e., in solution processed bilayer devices, comprising a layer of P3HT and a top-layer of HV-BT. The optimized device exhibited a power-conversion efficiency of close to 1%, and the efficiency of such cells was mainly determined by the device architecture [51].

Another interesting solution-based deposition method used to obtain thin films is the electrostatic layer-by-layer (LBL) adsorption technique, in which molecular-level control can be achieved. This technique was used to assemble thin films of PP and PC combined with several different organic molecules [54–58] and inorganic nanoparticles [59–63]. Although the properties of these films are usually well characterized, only a few reports can be found showing the use of these materials in photovoltaic devices.

Ultrathin films serving as a light-harvesting and hole transporting materials were fabricated via LBL deposition of the water-soluble copper(II) phthalocyanine-3,4',4'',4'''-tetrasulfonic acid tetrasodium salt (CuPCTS) and poly(diallyldimethylammonium chloride) (PDDA) [64]. The absorption characteristics of these films

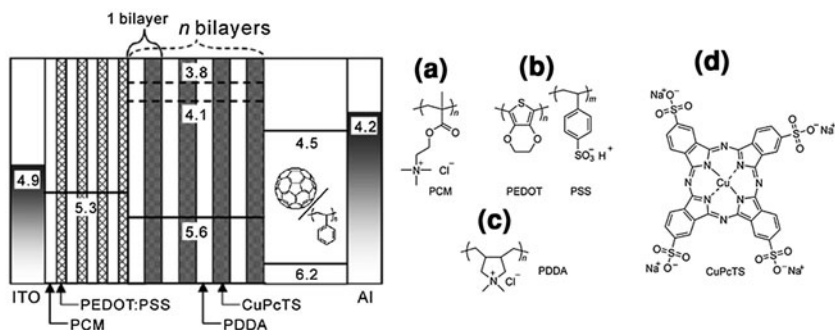


Fig. 11 Illustration of the photovoltaic cell with a triple-layered structure ITO/PCM/PEDOT:PSS/(PDDA/CuPcTS)*n*/C₆₀/Al. The thickness of PCM/PEDOT:PSS layer was 100 nm (20 bilayers) and C₆₀ layer was 50 nm, which were prepared by LBL deposition of PCM and PEDOT:PSS, and spin-coating from the blend solution of C₆₀: PS (4: 1 wt%) in *o*-dichlorobenzene, respectively. The thickness of PDDA/CuPcTS layer was varied from 0 (*n* = 0) to 14.4 nm (*n* = 6). Numerical values represent the Fermi-level energies for ITO (4.9 eV), PEDOT:PSS (5.3 eV), Al (4.2 eV), and HOMO and LUMO levels for CuPcTS (5.6 and 3.8–4.1 eV), and C₆₀ (6.2 and 4.5 eV). The chemical structures of polyelectrolytes used in the LBL deposition: **a** PCM (polycation), **b** PEDOT:PSS (polyanion), **c** PDDA (polycation), and **d** CuPcTS. “Reprinted from Bente et al. [64], copyright (2009), with permission from Elsevier.” (<http://www.sciencedirect.com/science/journal/00406090>)

indicated that the CuPcTS forms dimers or oligomers, and their molecular planes were oriented parallel to the substrate. Triple-layered OSCs were developed by combining CuPcTS with a poly(3,4-ethylenedioxythiophene):polystyrenesulfonate (PEDOT:PSS) hole-transport layer and a C₆₀ electron-transport layer, displayed in Fig. 11. The J_{SC} increased with increasing CuPcTS film thickness up to ca. 10 nm, as a result of exciton generation in each CuPcTS layer and transport to the interface with the C₆₀ layer. The best J_{SC} value of 0.114 mA cm⁻² reported is low compared to devices assembled using other solution processing methods and is probably caused by a poor light absorption inherent from the small layer thicknesses.

Generally, the photocurrent of devices assembled using the LBL technique are still on the order of microamperes, but the self-assembly properties obtained using this technique might be very useful for the future development of well-organized and highly efficient devices.

3 Evaporated Small Molecules OSC

3.1 Growth Techniques

Among the various growth techniques capable of producing thin films of small-molecular weight materials for OSCs, two techniques deserve special attention: vacuum thermal evaporation (VTE) [65] and organic vapor-phase deposition

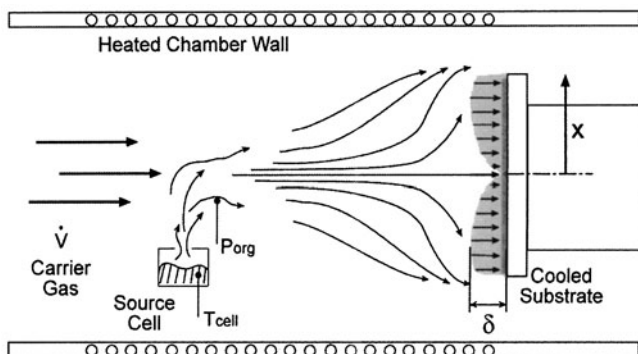


Fig. 12 Schematic diagram of the OVPD method. Organic materials are first evaporated into a carrier gas stream, which transports the molecules toward a cold substrate, where the vapor condenses into a solid film. When the substrate is rotated, the thickness of the boundary layer becomes uniform. “Reprinted with permission from Shtein et al. [66]. Copyright [2001], American Institute of Physics”

(OVPD) (Fig. 12) [66]. Thermal sublimation in vacuum is the most frequently used means for depositing small molecules that are insoluble in the majority of solvents [65]. The VTE procedure involves placing a purified organic material in a baffled tantalum or tungsten boat which is located between the electrodes in a vacuum chamber with a pressure of 10^{-6} – 10^{-7} Torr. When current is passed through the boat or crucible, the temperature is increased beyond the sublimation point of the organic material, and it is evaporated, depositing everywhere on the chamber walls, as well as on the target substrate. A quartz crystal microbalance is used to monitor the growth rate (typically 0.5 – 3 \AA s^{-1}) and the thickness of the film. VTE has the advantage of being able to form films with high uniformity, high degree of purity, good structural control, and “run-to-run” reproducibility. Additionally, one particular advantage of VTE is its ability to grow several OS layers without delamination or dissolution of the previous layers during subsequent deposition steps [67]. However, this technique presents several drawbacks such as lack of control over film thickness, uniformity, and dopant concentration over large areas needed for many applications. Moreover, this technique requires a relatively high material consumption and the initial setup costs for equipment are also very high.

To overcome the drawbacks associated with the VTE technique, OVPD was introduced as an alternative method for depositing thin films of small molecular weight materials and allowed greater control over doping. Besides, this technique is suitable for fast, particle-free, uniform deposition in large-area substrates [66, 68].

The process of OVPD differs from VTE; here the organic material is thermally evaporated into an inert gas stream such as nitrogen or argon, which then transports the vapor in the hot-walled reactor vessel and toward a cooled substrate where deposition occurs [69]. In this respect, OVPD allows one to adjust multiple

parameters such as reactant concentration, carrier gas flow rate, deposition rate, substrate temperature, chamber temperature, and chamber pressure. Thus, the deposition efficiency and film morphology are controlled [70, 71].

In this technique, the heated chamber walls avoid material deposition, allowing for a more efficient use of source materials compared with VTE [72]. Even with such differences, both VTE and OVPD techniques are used to manufacture OSCs based on small molecules [73, 74]. In the next section, different types of solar cell architectures using evaporated small molecules and recent results from many research groups are presented.

3.2 Organic Solar Cells Architectures

Besides manipulating the chemical and physical properties of small molecules, the choice of the growth technique and the selection of the best donor and acceptor combination are also important factors in controlling the device's architecture. These additional factors should be taken into account when attempting to improve the performance of solar cells [72]. In the next section, several device architectures using small molecules are described, highlighting the most important contributions in this field.

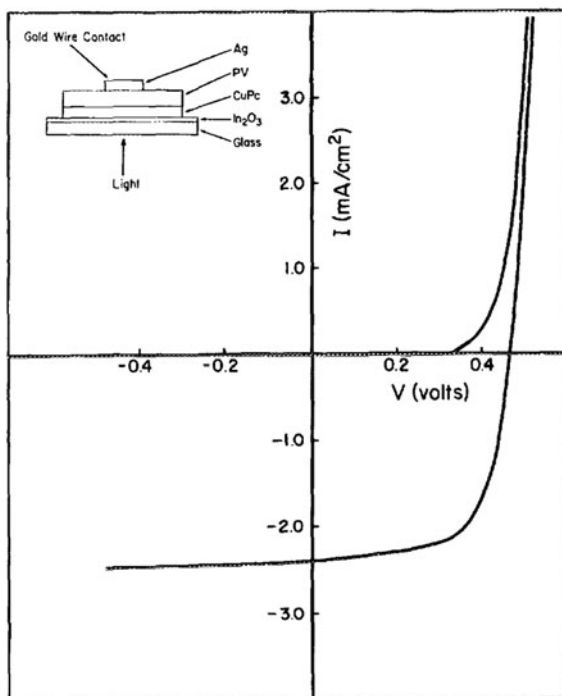
3.2.1 Double-Layer Solar Cells

The first successful OSC to reach a power-conversion efficiency of 1% was introduced by Tang at Kodak in 1986 [29]. Tang's solar cell consisted of a double layer of ~ 300 Å copper phthalocyanine (CuPC) as the electron-donating material and perylene tetracarboxylic derivative (~ 500 Å), as the electron-accepting material. Both materials were deposited by sequential thermal evaporation onto an indium tin oxide (ITO) substrate. On top, an opaque Ag layer was evaporated (Fig. 13). One of the most important conclusions derived from Tang's experiment is that the increase in thickness of the organic material layers led to a reduction in efficiency. Hence, the authors inferred that only excitons generated in the proximity of the interface between the donor and the acceptor materials were able to generate free charge carriers. Such a phenomenon reflected on the values of J_{SC} .

In the work reported by Tang, different metal contacts such as In, Al, Cu, and Ag were tested in the role of a top electrode. These metals, with different work functions produced solar cells with V_{OC} values differing by only 50 mV. It was assumed that V_{OC} is strongly dependent on the choice of the particular pair of organic layers.

Aiming to improve the efficiency of OSC, the group of Prof. Forrest [75] introduced an additional layer of bathocuproine (BCP) in double heterojunction solar cells. In this pioneering work, evaporated films of CuPC and 3,4,9,10-perylenetetracarboxylic *bis*-benzimidazole (PTCBI) were employed as the electron

Fig. 13 Device configuration and current–voltage characteristics of an ITO/CuPC (250 Å)/perylene tetracarboxylic derivative (450 Å)/Ag solar cell. “Reprinted with permission from Tang [29]. Copyright [1986], American Institute of Physics”



donor and acceptor, respectively. The BCP and Ag cathode were also evaporated and the final cell architecture was ITO/CuPC/PTCBI/BCP/Ag. 2.4% efficient solar cells were produced using this double heterojunction approach. This device architecture demonstrates that the control over the exciton diffusion can lead to a significant increase in the number of charge carriers. One year after this work, the same group reported an external power-conversion efficiency of 3.6% employing the same architecture [32]; here, the acceptor molecule was replaced by C_{60} . Both reports highlighted the strong influence of BCP in these devices.

The introduction of BCP molecule represents one of the greatest advances in small molecule-based solar cells assembly by evaporation techniques. This wide band gap molecule acts as an exciton blocking layer (EBL) between the electron acceptor material and the cathode, as shown in Fig. 13.

The HOMO–LUMO offsets between the acceptor and the BCP provide reflection of excitons at the interface of these materials, preventing recombination [75]. In this context, Vogel et al. [76] presented a detailed PL study on the function of the BCP layer insertion in small-molecule solar cell (Fig. 14a). In the case of sample 1, the weak PL was attributed to the fast nonradiative recombination (i.e., exciton quenching) at the Al- C_{60} interface. In contrast to sample 1, significant PL was observed in sample 2, clearly showing the PL spectrum of the C_{60} . Sample 3, containing a BCP layer between C_{60} and Al, showed the strongest PL and consequently the lowest exciton quenching yield. These results corroborate

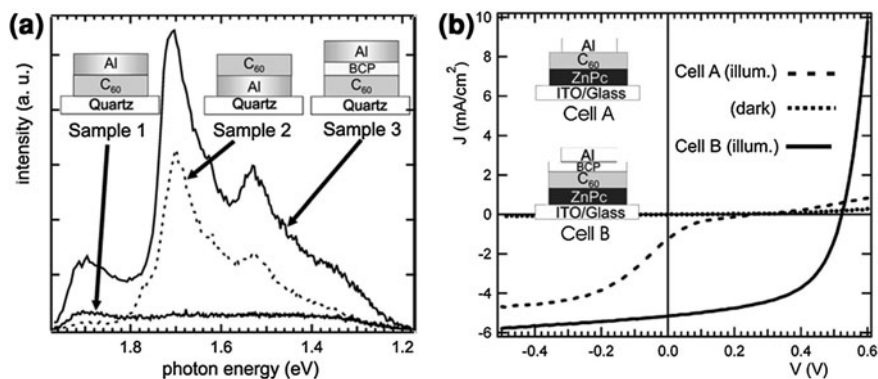


Fig. 14 **a** Photoluminescence spectra of C_{60} films at 10 K with different interfaces with Al. The direction of excitation and PL is indicated in the *inset* sample schemes. **b** Current density–voltage characteristics of photovoltaic cells with sequentially deposited ZnPC and C_{60} films with and without BCP buffer layer. Photovoltaic cell parameters are the following: cell A: $J_{SC} = 1.2 \text{ mA cm}^{-2}$, $V_{OC} = 0.12 \text{ V}$, $FF = 0.12$, and $\eta = 0.0\%$; cell B: $J_{SC} = 5.2 \text{ mA cm}^{-2}$, $V_{OC} = 0.52 \text{ V}$, and $FF = 0.5$, and $\eta = 1.5\%$. “Reprinted with permission from Vogel et al. [76]. Copyright [2006], American Institute of Physics”

previous reports that BCP may in fact be preventing exciton recombination at the Al- C_{60} interface [76].

Vogel et al. [76] further analyzed the function of BCP layer by interpretation of the photocurrent–voltage (J – V) in double-layer photovoltaic cells. Two types of devices were prepared using zinc phthalocyanine (ZnPC) as the donor and C_{60} as the acceptor, with and without BCP layers. These devices are represented by cell A and cell B in Fig. 14b, respectively. The short-circuit current density (J_{SC}) was reduced from 5.2 mA cm^{-2} in cell B to 1.2 mA cm^{-2} in cell A. In contrast, at a bias of -0.5 V , the photocurrent in cell A is only about 20% lower. Such strong dependence of the photocurrent on the voltage shows that exciton quenching explains only a small part of the photocurrent loss in cell A, since excitons are neutral and therefore independent of applied bias. Important theoretical calculations of electric field distribution and exciton diffusion were carried out by Breyer et al. [77]. The authors show that even complete quenching of excitons at the Al- C_{60} interface does not reduce the photocurrent by more than about 13% compared to an exciton-reflecting interface. Therefore, the larger part of the photocurrent increases in cell B is mainly attributed to the improved efficiency of electron transport from C_{60} to the Al electrode via the BCP layer. In other words, the most important function of BCP is to establish an Ohmic contact between Al and C_{60} .

BCP has been typically used as an EBL material in small molecule-based solar cells. However, its large energy gap and low conductivity make it unsuitable for use in thick layer devices because the increase in the series resistance degrades device’s performance.

Interestingly, Rand et al. [41] introduced an EBL composed of *tris*(acetylacetonato) ruthenium(III) ($\text{Ru}(\text{acac})_3$). Its functionality results from an energy-level

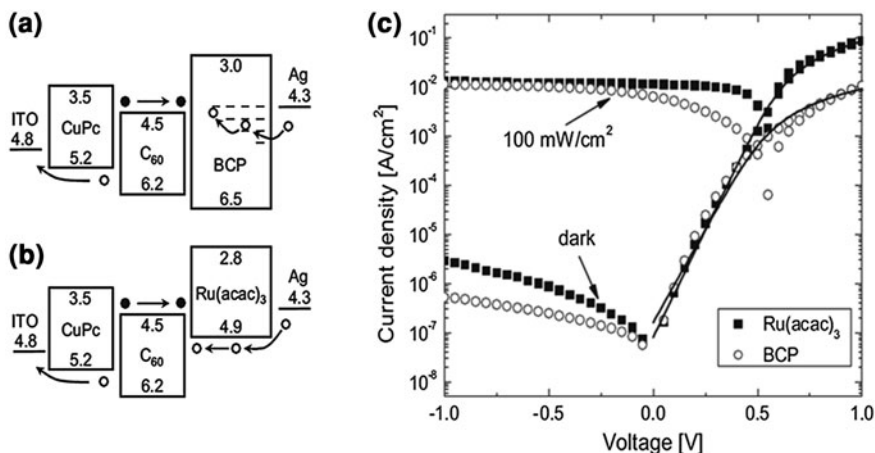


Fig. 15 Schematic energy-level diagram and proposed photovoltaic process for double-heterostructure devices using either **a** BCP or **b** Ru(acac)₃ EBL. Holes are shown as *open circles* and electrons as *filled circles*. Energy levels are given in units of electron-volts (eV). **c** Current-density–voltage (J–V) characteristics, in the dark and under 1 sun (100 mW cm^{−2}) intensity of simulated AM1.5G, for the organic photovoltaic cells with the following structure: ITO/CuPC(200 Å)/C₆₀(400 Å)/EBL(200 Å)/Ag(1000 Å). The EBL consists of either BCP (*open circles*) or Ru(acac)₃ (*filled squares*). The efficiencies for BCP and Ru(acac)₃ based devices are 1.1 and 2.7%, respectively. The *solid lines* are fits to the J–V characteristics based on the modified ideal diode equation (Rand et al. [41]). Copyright Wiley–VCH Verlag GmbH & Co. KGaA. Reproduced with permission

alignment more favorable than BCP, as seen in Fig. 15a, b. This is reflected in the remarkable differences observed in photocurrent–voltage characteristics as shown in Fig. 15c.

3.2.2 Bulk-Heterojunction Solar Cells

The DA interface can be considered to be the heart of the small-molecule solar cells. It is at this interface that strongly bound photogenerated excitons are dissociated to generate photocurrent. The external quantum efficiency (η_{EQE}) of a photovoltaic cell based on exciton dissociation at a DA interface is $\eta_{\text{EQE}} = -\eta_{\text{A}} \times \eta_{\text{ED}} \times \eta_{\text{CC}}$ [78], where η_{A} is the absorption efficiency, η_{ED} is the exciton diffusion efficiency that corresponds to the fraction of photogenerated excitons that reach the DA interface before recombining, and η_{CC} is the carrier collection efficiency and corresponding to the probability that a free carrier, generated at a DA interface by dissociation of an exciton, reaches its corresponding electrode. When the total thickness, L , in bilayer DA solar cells is of the order of the optical absorption length, L_{A} , we can assume η_{A} , described in Eq. 1 [78], to be higher than 50% if optical interference effects are ignored, and $\eta_{\text{CC}} \approx 100\%$. Nevertheless, since the exciton diffusion length (L_{D}) is typically

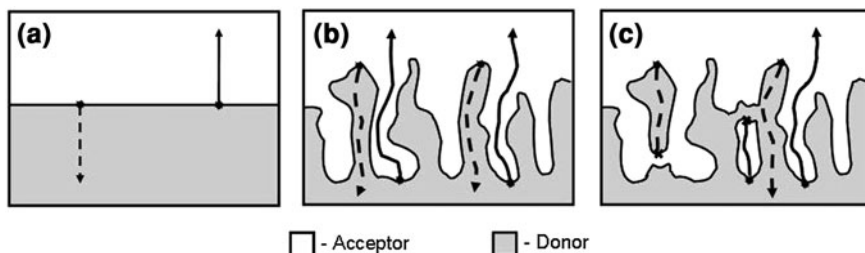


Fig. 16 Representation of donor/acceptor interface architecture possibilities: **a** a double layer, formed between thin films of donor and acceptor materials; **b** an optimal bulk heterojunction, where there is complete phase separation of donor to one side and acceptor to the other side of the device structure; and **c** a non-ideal bulk heterojunction, where isolated regions of donor and/or acceptor phases prevent the collection of photogenerated charges. *Dashed and solid lines* correspond to hole and electron transport, respectively

an order of magnitude smaller than L_A , a large fraction of the photogenerated excitons are not used for photocurrent generation as shown in Fig. 16. Therefore, limited η_{EQE} and hence limited η are observed for double-layer solar cells.

$$\eta_A = 1 - \exp(-L/L_A) \quad (1)$$

The η_{EQE} of an organic double-layer solar cell is often limited by a short exciton diffusion length. To overcome this drawback, the bulk-heterojunction concept has been introduced [78–82], resulting in an improvement in both η_{EQE} and in the η .

Bulk or mixed heterojunction is a mixture of the donor and acceptor materials in a bulk volume, exhibiting a DA phase separation of about 10–20 nm which provides an interpenetrating DA network with large interface area [83]. Compared with the planar double layer cells introduced by Tang, in which the donor and acceptor phases are completely separated from each other (Fig. 16a), the bulk heterojunction has both materials intimately intermixed. It expands the photocurrent generation capability of the device by increasing the excitons' probability of reaching a nearby DA interface where they can dissociate [72].

In polymer photovoltaic cells, the exciton diffusion bottleneck has been overcome by the introduction of bulk heterojunctions [84, 85] (Fig. 16c). In a bulk heterojunction, the DA interface is highly folded so that photogenerated excitons can find an interface within a distance L_D of their generation site. In an optimal architecture [86], the width of the phases in the interdigitated structure should be on the order of $2L_D$ to guarantee high probability of dissociation for the excitons generated in the bulk of the material. At the same time, this optimal architecture provides low resistance pathways for charge transport. In practice, however, achieving such a structure is difficult. Recently, optimized polymer bulk-heterojunction cells have reached power-conversion efficiency of 7% [87]. In this work, a blend of a novel semiconducting polymer based on alternating ester substituted thieno[3,4-b]thiophene and benzodithiophene units and PC₇₁BM. The polymer

exhibits a low bandgap, providing an efficient absorption around the region with the highest photon flux of the solar spectrum (about 700 nm). The rigid backbone results in a high hole mobility, and the side chains on the ester and benzodithiophene enable good solubility in organic solution and suitable miscibility with the fulleride acceptor. The polymer chain is found to be stacked on the substrate in the face-down conformation from grazing-incidence wide-angle X-ray scattering studies. This is very different from the polymer alignment in well-studied P3HT solar cell system and favors charge transport [87]. This synergistic combination of properties lead to an excellent photovoltaic effect (and efficiency record!).

Remarkable efforts have been conducted to perform bulk-heterojunction devices prepared by co-deposition of the donor and acceptor materials yielding η values falling short of those attainable in optimized bilayer cells using the same materials [32, 79, 82, 88–91]. Co-deposited donor and acceptor small molecules have been used to prepare bulk-heterojunction photovoltaic devices [78, 80, 92–96] reaching power-conversion efficiency of approximately 3.5%. Using this approach, the deposition of the mixed donor and acceptor phase is usually followed by a decrease in charge-carrier mobility, i.e., by an increase in the series resistance (R_S) of devices [92, 97]. This behavior is different from that observed in polymer bulk-heterojunction structures [98]. The charge-carrier mobility is critically dependent on the composition and morphology in both polymer and small molecule bulk-heterojunction structures. From space charge limited current mobility measurements, Rand et al. [92] demonstrated that mixed layers presented lower charge-carrier mobilities than neat films.

Aiming to accomplish a nearly ideal structure in the thermally co-evaporated thin film, Peumans et al. [78] carried out an annealing treatment of the CuPC:PTCBI mixture (300–500 K). Such post-treatment was responsible for inducing phase separation of the two materials and an increase in η_{CC} .

Donor and acceptor mixed layers can also be deposited via the OVPD growth technique to directly form a bulk-heterojunction architecture in which the two layers are phase-separated [99] (Fig. 16b). By this method, it is possible to control the growth mode of the CuPC film on ITO such that, crystalline needles of CuPC extend out of the CuPC film. After growth of the CuPC film, the OVPD process was successfully applied to fill the spaces within the rough CuPC film. This contrasts with growth induced by ultra high vacuum, in which the VTE process results in voids in the film [99] (Fig. 16a). This architecture resulted in an increase in device efficiency of the CuPC/PTCBI solar cell from 1.1 to 2.7%. The photovoltaic parameters for all architectures based on ITO/CuPC/PTCBI/BCP/Ag solar cells are shown in Table 1.

Achieving a balance between the absorption needed for photocurrent generation and a good charge transport in bulk-heterojunction devices is challenging. Therefore, maintaining a good charge transport and a low R_S are important factors in creating efficient OSCs [100] with high FFs, and reduced recombination probability of the photogenerated charges within the mixture. This can be achieved using a hybrid architecture: combined double layer and bulk heterojunction approaches. This configuration consists of a bulk-heterojunction DA layer

Table 1 Comparison of performance of several ITO/CuPC/PTCBI/BCP/Ag photovoltaic cell structures characterized under 1 sun simulated AM1.5G illumination

Device	J_{SC} (mA cm ²)	V_{OC} (V)	FF	η (%)	R_S (Ω cm ²)
Double layer using VTE ^a	6	0.49	0.49	1.1 ± 0.1	30 ± 10
Annexed bulk hetero junction ^b	9	0.50	0.40	1.4 ± 0.1	60 ± 10
Double layer using OVPD	5	0.4S	0.47	1.1 ± 0.1	18.2 ± 0.5
Controlled bulk OVPD heterojunction	11	0.49	0.58	2.7 ± 0.1	2.2 ± 0.1

R_S is the specific series resistance [99]

^a Ref. [75]

^b Ref. [78]

Table 2 Comparison of several OSC using different architectures, under approximately 1 sun simulated AM 1.5G illumination, where P_0 is the incident optical power density [101]

Device	P_0 (suns)	J_{SC}/P_0 (mA W ⁻¹)	FF	V_{oc} (V)	η (%)
Double layer ^a	1.3	11.8 ± 0.5	0.61	0.51	3.7 ± 0.2
Bulk heterojunction ^b	0.9	15.4 ± 0.7	0.46	0.50	3.5 ± 0.2
Double layer/bulk heterojunction	1.2	15 ± 0.6	0.61	0.54	5.0 ± 0.3

^a Ref. [100]

^b Ref. [93]

sandwiched between homogeneous donor and acceptor layers [101]. Because each homogeneous layer has a thickness of approximately L_D , excitons are generated in the entire heterojunction structure with a high probability of diffusing to a nearby DA interface. This architecture provides both high η_{ED} of a bulk heterojunction and efficient charge collection characteristic of a double-layer device [101].

Using this approach, Xue et al. [101] fabricated solar cells consisting of the donor CuPC, and acceptor C₆₀, obtaining a power-conversion efficiency of 5% under 1–4 sun of simulated AM1.5G illumination. The authors also compared these devices with the bulk heterojunction and double-layer solar cells. The photovoltaic parameters of these solar cells are summarized in Table 2. Remarkably, this innovative concept afforded an increase in FF values and further resulted in efficient charge transport in the active layer.

3.2.3 Tandem Solar Cells

In solar cells with only one band gap, the Shockley–Queisser limit [102] can be reduced due to mainly two loss mechanisms [103]: thermalization losses and losses via sub-band gap transmission of photons. Aiming to overcome these limitations, tandem or multi-junction architectures have been investigated and appear to be promising solutions. When two or more donor materials with non-overlapping absorption spectra are used in a tandem solar cell, a broader range of the solar spectrum can be covered. In the last years, several approaches for organic

tandem cells have been employed, depending on the materials used for the active layer and the separation or recombination layer(s). In general, these approaches can be divided in three main categories: (i) tandem OSCs where both the bottom (in front of the light illumination) and the top (back) cells are based on small molecules growth by vacuum-deposition techniques; (ii) hybrid tandem OSCs in which the bottom cell is processed from solution while the top cell is made of vacuum-deposited small molecules; and (iii) fully solution-processed tandem OSCs where both the bottom and top cells are deposited from solution. In this section, only the first approach will be described, together with some promising results described recently in the literature.

The use of small molecules presents a great advantage for tandem architectures because different layers of donor and acceptor (or mixed layer) materials can be evaporated or co-evaporated with sharp interfaces on top of each other, without affecting the previously evaporated layer. The disadvantage, however, comes from the relative low evaporation rate of active materials, which limits the processing speed in large-area applications [104].

Tandem solar cells can theoretically be comprised of an infinite number of sub-cells connected in series. According to Kirchhoff's law, this type of connection implies that the voltage across the entire cell is equal to the sum of the voltage across each sub-cell. The V_{OC} of these devices containing series sub-cells, in the case of loss-free connections, is given by [105, 106]:

$$V_{OC,tot} = V_{OC1} + V_{OC2} + V_{OC2} + K \quad (2)$$

On the other hand, on contrary to what is often mentioned, the short-circuit current of the organic tandem solar cells is not equal to the smallest short-circuit current of the sub-cells, but depends strongly on the FF values of the respective devices [106]. This behavior, illustrated in Fig. 17a, results in the combination of a cell with lower J_{SC} and a significantly higher FF and a cell with higher J_{SC} and extremely low FF. According to Kirchhoff's law, a $J-V$ characteristic of the tandem cell with a $J_{SC} = \text{Min}(J_{SC1}, J_{SC2})$ is attained. Oppositely, Fig. 17b shows the combination of a cell with extremely low FF and lower J_{SC} and another with very good FF and higher J_{SC} , leading to a resultant tandem device with a $J_{SC} = \text{Max}(J_{SC1}, J_{SC2})$. A description of the various cases was presented by Hadipour et al. [105].

The tandem cell architecture was originally introduced by Hiramoto et al. [107]. This architecture was constructed from two identical bilayers based on evaporated small molecules, where each bilayer was an organic DA junction consisting of 50 nm of metal-free phthalocyanine (H_2PC) and 70 nm of perylene tetracarboxylic derivative. These two bilayers were separated by a thin interstitial layer (2 nm) of Au, in order to establish an Ohmic contact. The organic tandem cell resulted in almost double the V_{OC} (0.78 V) compared to single cell, in which the V_{OC} was 0.44 V. This result showed that a thin interstitial Au layer was able to accomplish an effective charge recombination site for electrons arriving from the perylene tetracarboxylic derivative of the back cell with the holes coming from the H_2PC of

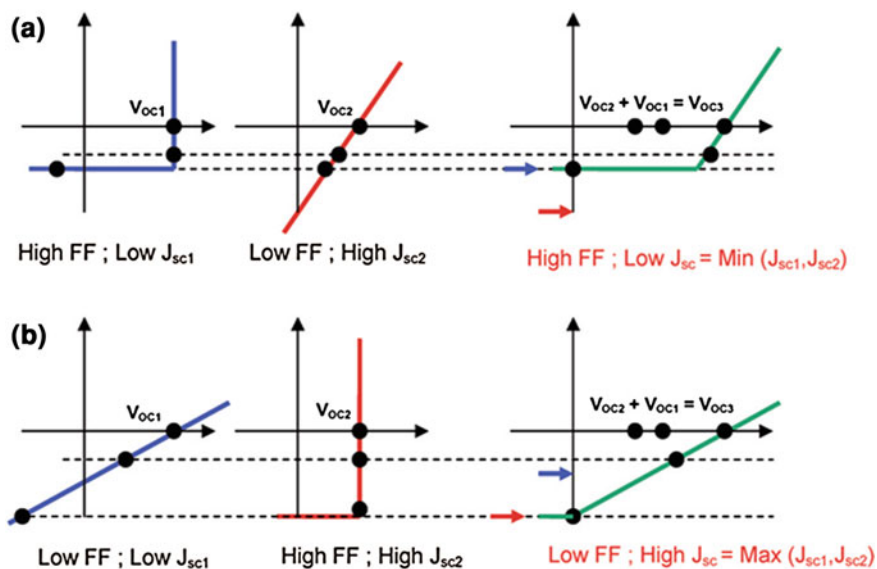


Fig. 17 **a** The combination of a cell with lower J_{SC} and significantly higher FF and a cell with higher J_{SC} and extremely low FF results in a tandem cell with a $J_{SC} = \text{Min}(J_{SC1}, J_{SC2})$. **b** The combination of a cell with extremely low FF and lower J_{SC} and another with very good FF and higher J_{SC} leads to a tandem device with a $J_{SC} = \text{Max}(J_{SC1}, J_{SC2})$. Ameri et al. [106]—reproduced by permission of The Royal Society of Chemistry

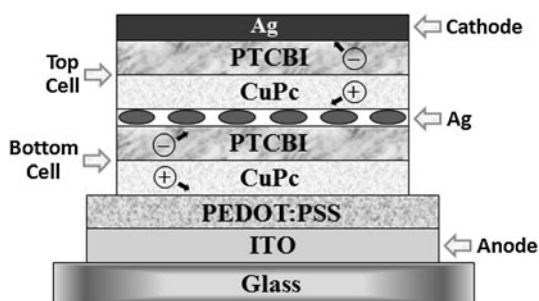
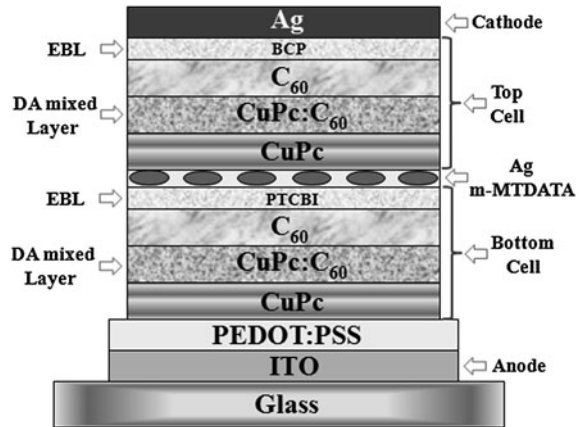


Fig. 18 Schematic structure of an organic tandem solar cell based on the small molecules CuPc as donor and PTCBI as acceptor performed by Yamikov and Forrest [109]. The 0.5 nm Ag separation layer provides recombination sites for the electrons and holes (<http://dx.doi.org/10.1039/B817952B>)

the front cell. In general, this interstitial layer is sufficiently thin to efficiently supply charge recombination sites, and also is not thick enough to absorb light on its way to the back cell, nearest the reflecting cathode [108].

Yamikov and Forrest [109] reported in 2002 the first tandem solar cells by stacking two, three, or five vacuum-deposited thin heterojunction consisting of

Fig. 19 Schematic structure of hybrid double-bulk-heterojunction organic tandem solar cell



CuPC, as donor, and PTCBI, as electron acceptor. Between the DA bilayers, a thin layer of Ag was deposited providing the charge recombination sites. The final structure can be seen in Fig. 18.

The power-conversion efficiencies reached by the two and three-stacked solar cells were $\eta = 2.5\%$ and $\eta = 2.3\%$, with $V_{OC} = 0.93$ and 1.2 V, respectively. These values are twofold higher compared to a single junction cell based on identical materials ($\eta = 1.1\%$). Rand et al. [110] found that the optical field enhancement, due to surface plasmon generation on the metal clusters located at the interstitial layers, was responsible for the higher efficiency. In contrast, the five stacked cell showed a considerable decrease in η (1%) compared to devices containing two or three-stacked bilayers. This observation comes from the reduction in light absorption by the first bilayers, that being the main limitation of multiple-heterojunction solar cells. Triyana et al. performed similar approach using CuPC and PTCBI as donor and acceptor materials, respectively, in combination with ultrathin Ag and Au interlayers to produce multiple-junction solar cells with two and three stacks [111, 112].

To improve the power-conversion efficiency in tandem solar cells, Xue et al. [113] applied several modifications to the device's structure. The use of C_{60} as acceptor materials, with a longer exciton diffusion length ($L_D \sim 40$ nm) compared to the acceptor PTCBI [114], is the first modification. The second is the use of an evaporated mixed DA layer or bulk-heterojunction structure sandwiched between neat donor and acceptor layers. Thin layers of PTCBI and BCP were employed as EBLs in the bottom and top sub-cells, respectively. These modifications gave rise to a highly efficient double bulk-heterojunction structure. It was suggested that one EBL may be acting as a protection for the hot metallic particles during the thermal evaporation process. In such device, ultrathin Ag interstitial layer are recombination site which have a thickness of 5 \AA buried in a 50 \AA thick 4, 4', 4''-tris(3-methyl-phenyl-phenyl-amino)triphenylamine (*m*-MTDATA) p-doped with 5 mol% tetrafluoro-tetracyano-quinodimethane. This structure with a mixed DA layer sandwiched between homogenous donor and acceptor layers is named hybrid

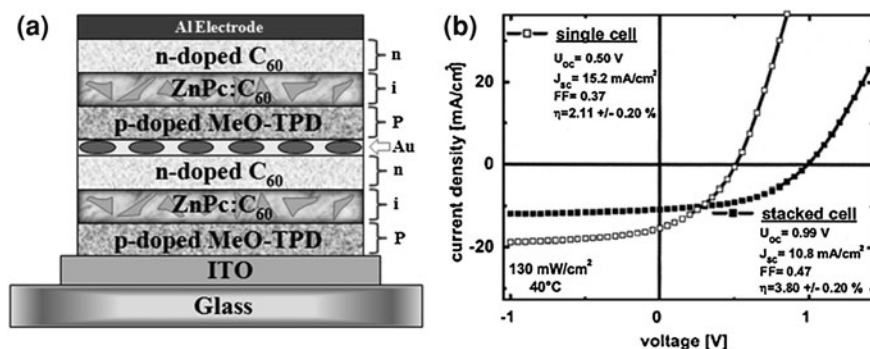


Fig. 20 **a** Concept of a stacked p–i–n OSC with active layers sandwiched between p- and n-type wide-gap transport layers. **b** J–V characteristics of single and tandem p–i–n solar cells under 130 mW cm^{-2} simulated AM 1.5 solar illumination. The single cell is identical to the bottom cell in the tandem configuration (Cell A) and prepared simultaneously. The performance parameters are given. “Reprinted with permission from Drechsel et al. [115]. Copyright [2005], American Institute of Physics”

double-bulk heterojunction [101, 113], and is schematically represented in Fig. 19. Another important finding concerns the effect of different layers thickness that resulted in 5% efficiency. It demonstrates the undercover potential of such approach and that the device’s optimization may even augment the efficiency value.

Drechsel et al. [115] introduced an effective means to space the sub-cells apart by employing a p–i–n heterojunction architecture, as depicted in Fig. 20. In this case, the *N,N,N',N'*-tetrakis(4-methoxyphenyl)-benzidine (p-doped MeO–TPD) and the n-type C_{60} wide-gap transport layers (which optimally do not absorb the incident light) are used to spatially separate the mixed ZnPC: C_{60} (i-type materials) layers that generate photocurrent.

The photocurrent–voltage characteristics for the single and tandem p–i–n solar cells are shown in Fig. 20b. The power-conversion efficiency is 2.1% for the single device and 3.8% for the tandem cell. It is very common to observe that optimized organic tandem cells have lower J_{SC} values than optimized single cells.

More recently, Yu et al. [116] assembled organic tandem solar cells without metallic nanoclusters between the sub-cells. In contrast, they fabricated organic tandem cells employing all-organic units by continuous deposition. These all-organic connecting units were heterojunction films, which have a better transparency and a lower sublimation temperature than Au or Ag. A tunneling mechanism was suggested as an explanation to why the organic heterojunction became an effective charge recombination center. In an optimized tandem solar cell comprising a tin phthalocyanine dichloride (SnCl_2PC)/copper hexadecafluorophthalocyanine (F_{16}CuPC) heterojunction as the connecting unit, the V_{OC} is almost twice that as a sub-cell, reaching up to 1.04 V, and 60% enhanced IPCE ($\eta = 1.8\%$). Furthermore, the all-organic connecting units can be continuously

deposited, which provides an easy way to fabricate these devices and avoids damage to the organic films.

4 Liquid Crystals

If the nanomorphology of the active layer could be controlled on a molecular scale, the efficiency of charge separation and transport would be expected to increase substantially, improving the performance of these devices. Since most organic photovoltaic materials are amorphous solids or polymers with limited charge mobilities and exciton diffusion lengths, an approach to achieve the necessary enhancement in efficiency is the use of self-assembled materials into large domains of crystalline or liquid crystalline order. In this context, the use of discotic liquid crystalline materials and composites might reach this goal because of their capacity to self-organize into columnar stacks, maintaining high charge-carrier mobility while providing a well-distributed interface between the donor and acceptor semiconductors.

The supramolecular assemblies of aromatic disc-shaped molecules, which lead to the formation of discotic LCs, were discovered in 1977 by Chandrasekhar and colleagues [117]. These disc-shaped molecules exhibit liquid crystalline properties at room temperature (RT), with LC to liquid transition (clarification) temperatures (CT) usually above 150°C. The discotic molecules generally consist of an aromatic core surrounded by aliphatic chains. Due to strong π - π interaction between the cores and weak interaction between the flexible aliphatic chains, the molecules can stack one over the other, forming columns, when slowly cooled from above CT to RT. Thus, well-oriented large domains can be obtained. These columns can be arranged in several ways, forming columnar hexagonal, columnar rectangular, columnar oblique, columnar helical, or columnar plastic phases [118]. Typical column-column distance in the columnar hexagonal phase is 2–4 nm depending on the aliphatic chain length and the core-core distance within the column is around 0.35 nm with a length of a few tens of nanometers.

The strong intracolumnar interaction and weak intercolumnar interaction contribute to the quasi-one-dimensional electrical conductivity along the columns. Long exciton diffusion lengths (a few 100 nm) and high charge-carrier mobilities (up to $0.1 \text{ cm}^2 \text{ V}^{-1} \text{ s}^{-1}$) have been found in the highly ordered liquid crystalline discotic molecules [119]. The mobility along the columns is superior to typical mobility of amorphous organic films and can reach values found for amorphous silicon [120–122]. Provided the distance between the single discs is short, electrons and excitons readily move along the columnar axes. Both p-type discotic LC, such as triphenylene, dibenzopyrene, and hexabenzocoronene (HBC) (Fig. 21a–c), and n-type discotic LC, such as tricycloquinazoline, anthraquinone, and perylene (Fig. 21d–f), are known [123]. Moreover, liquid crystalline phases are self-repairing and thereby minimize defects that can act as recombination sites. While the aliphatic side groups affect the melting point, solubility, and film-forming

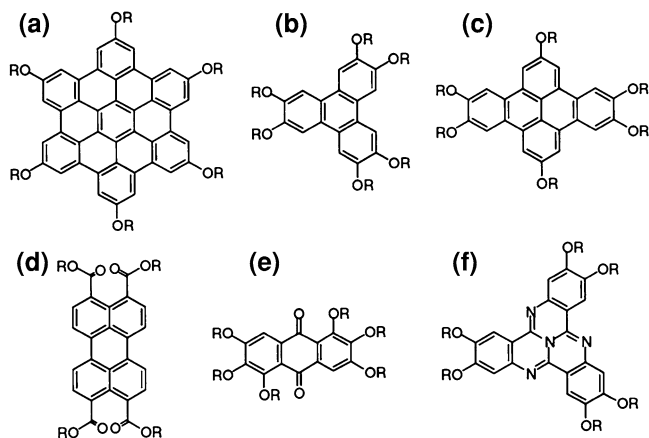


Fig. 21 Chemical structure of p-type (a–c) and n-type (d–f) discotics liquid crystals [123]

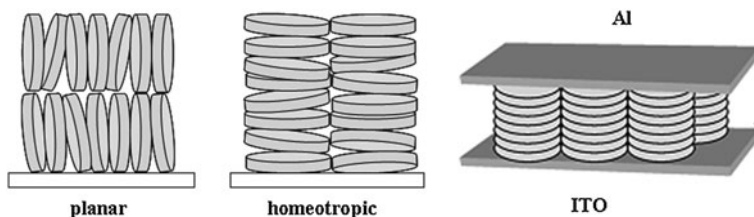


Fig. 22 Schematic representation of the planar (edge-on) and homeotropic (face-on) orientations of a columnar mesophase and ideal arrangements of the discotic stacks in a device configuration. The LC stacks should be perpendicular to the surface substrate and be surrounded by the electron-accepting material to obtain an ideal structure

properties, they have a negligible effect on the electrochemical oxidation/reduction potentials and optical properties, which depend on the core structure and the π -conjugation.

After the deposition of a LC molecule onto a substrate, the alignment can be planar (columns parallel to the substrate) or homeotropic (columns perpendicular to the substrate), as depicted in Fig. 22, depending on the type of the material, the substrate, and the experimental conditions (film thickness, cooling rate, etc.) [124]. Sometimes, after spin-coating or vacuum sublimation of a film with thickness below a critical value (typically a few hundred nanometers), the material clears upon heating to form an isotropic liquid that rapidly destabilizes into isolated droplets. This droplet formation can be avoided in many cases by an appropriate ITO surface treatment (e.g., annealing at high temperature) combined with a rapid cooling of the organic film through the liquid-to-LC phase transition [124, 125].

Grelet et al. [124] showed that uniform vertical orientation of the columnar axis on the substrate can be achieved in submicron open films by controlling the growth

kinetics of the columnar domains during thermal annealing. However, when the film thickness was reduced to the typical value required in OSC (50–100 nm), dewetting occurred, leading to inhomogeneous films. Later, the same group showed that by treating the substrate surface either by UV ozone or by nitrogen plasma, thin films of 50 nm of a columnar mesophase could be stabilized in homeotropic orientation on an ITO electrode [126].

HBC liquid crystalline derivatives have been widely used in efficient photovoltaic diodes [127]. The disk-like aromatic cores of HBC assemble face-on into columns, allowing for high charge-carrier mobilities along the discotic cores [128, 129]. The potential to form controlled, organized structures in optoelectronic devices is evident by the self-organization of HBCs in both “edge-on” heterotropic alignment [130] as well as homeotropic alignment perpendicular to the substrate [131].

The photovoltaic behavior of three hexa-*peri*-hexabenzocoronene derivatives with different-sized alkyl side chains was investigated [132]. Increasing the side chain length dilutes the HBC chromophore core, decreasing the amount of light absorbed by the film. Also, differential scanning calorimetry and X-ray analysis showed that, at RT, the HBC derivative with the 2-ethyl-hexyl side chain is in a crystalline state, while the HBC containing 2-hexyl-decyl or 2-decyl-tetradecyl substituents are in the so-called “plastic crystalline state”. The HBC with the shortest side chain was proven to be the best donor for perylenediimide, showing IPCE of 12% (at 470 nm).

Fluorenyl hexa-*peri*-hexabenzocoronene functionalized with a series of thiophene dendrons, were synthesized using the Suzuki–Miyaura coupling [133]. Ordered structures were observed in blends of these materials and fullerene acceptor materials. The larger thiophene dendritic substituent attached to the HBC derivative broadened its absorption profile, and also altered the morphology. A power-conversion efficiency of 2.5% was achieved for a device containing the compound depicted in Fig. 23a with PC₇₁BM as the acceptor material [133].

Schmidt-Mende et al. [134] built a photovoltaic solar cell using hexadodecylphenylhexabenzocoronene as the hole-transporting layer (Fig. 23b). A chloroform solution of this LC and the crystalline dye *N,N*(bis(1-ethylpropyl)-3,4,9,10-perylene-tetracarboxdiimide (PTCDI, Fig. 23c) was spin-coated onto ITO. PTCDI is a LC dye with a long chain hydrocarbon moiety bound to the nitrogen in the imide group, which self assembles in a similar manner to other perylene diimides [135]. The device exhibited IPCE up to 34% and power efficiencies of up to ~2%. The efficient photoinduced charge transfer and facile charge transport through vertically segregated perylene and HBC were considered responsible for the high efficiencies. The same group investigated later the performance of solar cells assembled with blends of perylene diimide and other HBC derivatives, spin-coated directly from solution [136]. The use of different HBC derivatives as hole conductors showed lower efficiencies, attributed to the different film morphology originated when spin-casting these materials.

In a different approach, Schmidtke et al. [137] employed the elastomer polydimethylsiloxane (PDMS) to control the film morphology and phase separation of

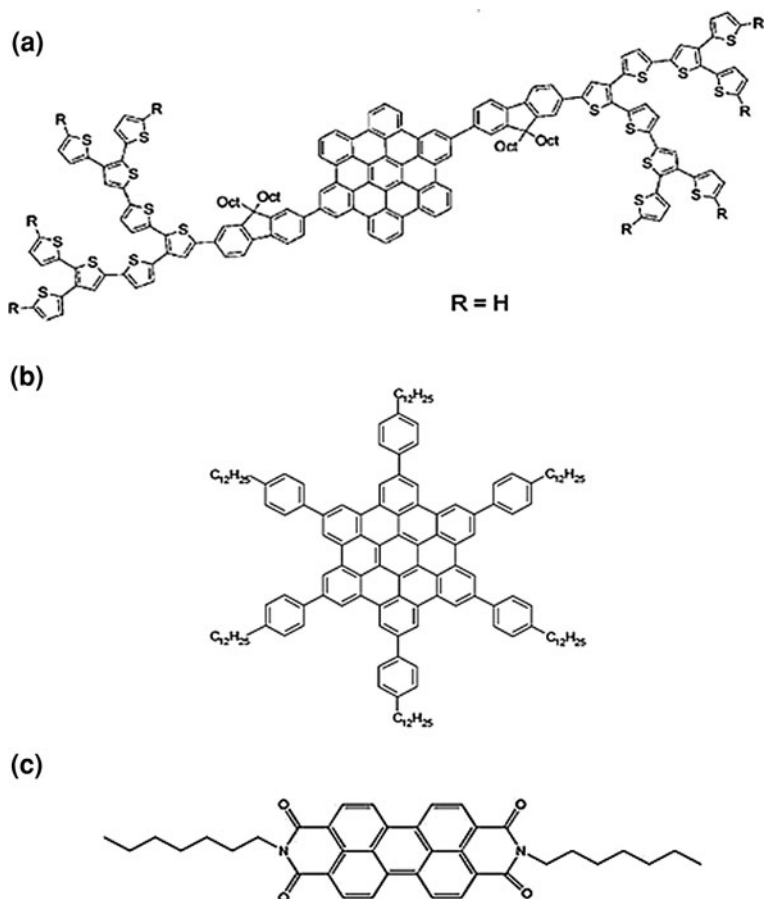
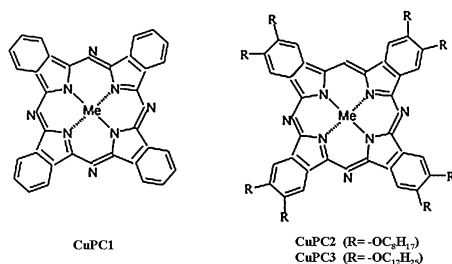


Fig. 23 Examples of HBC derivatives used as donors (a, b) and PTCDI dye used as an acceptor (c) in LC-based SPOSCs [133, 134]

blends containing PTCDI and hexadecylsubstituted-HBC. The PDMS stamp formed a flat, top-surface, which was utilized during the annealing step and then removed. The authors observed that the annealed devices showed a modest increase in IPCE compared to that of the as-spun devices, whereas the PDMS-annealed devices presented a twofold increase in IPCE over the as-spun films, reaching 29.5% at 460 nm. The AFM images showed different textures and patterns in each case. The annealing processes resulted in increased roughness and polycrystalline features, which suggest higher charge-carrier mobilities associated with the crystalline phases of the HBC derivative. Furthermore, the increased vertical stratification increased the V_{OC} in these devices [137].

Porphyrine-based molecules may also present liquid crystalline properties. Gregg et al. [138] studied in 1990 the photovoltaic effects of symmetrical cells

Fig. 24 Chemical structures of CuPC1, CuPC2, and liquid crystal CuPC3 [140]



filled with discotic liquid crystalline PP complexes. The authors did not study the charge mobility in the mesophase itself, but utilized the liquid crystalline properties to promote macroscopic order, which, upon cooling, provided polycrystalline films. In 1999, Petritsch et al. [139] fabricated a double-layer device using a liquid crystalline PC. They heated the PC until it reached its clarification point (292°C) and then cooled it slowly to RT. The films were fabricated in air by spin-coating from a chloroform solution. On top of the PC layer a thin layer of a perylene derivative was sublimated. The assembled devices presented efficiencies up to 0.5%.

Recently, Levitsky et al. [140] presented the preparation of a solar cell based on n-type nanoporous Si filled with copper phthalocyanine (CuPC1, in Fig. 24) and its derivatives (CuPC2, in Fig. 24), including a discotic LC form (CuPC3, in Fig. 24). The conversion efficiencies were between 0.01 and 0.02% (at 30 mW cm⁻²) when the CuPC-derivatives were used. For CuPC1, on the other hand, conversion efficiencies up to 2% were observed. The striking difference in conversion efficiency of hybrid devices was explained in terms of the interfacial area between organic and inorganic components. The critical factor in this case was believed to be the average distance between the CuPC core and the Si surface. The relatively long alkyl chains in CuPC2 and CuPC3 hindered the charge transfer in such a way that the LC organization in CuPC3 could not compensate for the low charge transfer caused by the long alkyl chains.

The properties of discotic LC can be modulated by doping with either electron-rich or electron-deficient molecules into the supramolecular, ordered phase. The doping should be kept at an optimum concentration while retaining the liquid crystalline phase and introducing sufficient electron or hole concentrations into the liquid crystalline medium to increase the conductivity. Trinitrofluorenone and several inorganic dopants, such as iodine, aluminum chloride, nitrosonium tetrafluoroborate and gold nanoparticles have been introduced in the columnar liquid crystalline matrix [141–145].

The versatility of LCs allows the application of these molecules in other types of solar cells as well, including silicon-based devices. For example, LC-based thermography has been successfully used for the investigation of various thermal phenomena in a wide range of applications, including the detection of shunts in polycrystalline silicon solar cells [146].

5 Ternary Component-Based OSC

For OSCs, effective absorption over a wide wavelength range is an important goal, which usually is not sufficient when using a simple DA pair. As an alternative, the inter or intralayer cascaded energy transfer concept has been proposed by Koeppel et al. [147] and Liu et al. [148], utilizing multiple photoactive materials in a single cell. The application of this method, however, is limited by the subtle balance of hole and electron mobilities in the bulk heterojunctions. Also, the interface formation and morphology are difficult to control in the presence of a third component in the active layer. In this section, recent reported results for three-component-based solar cells with small organic molecules are reviewed.

Figure 25a illustrates the basic ideas underlying the design of the multiple-heterojunction system with antenna effects: (i) a p–n heterojunction, containing an electron donor and an acceptor is responsible for exciton separation; (ii) antenna layers, i.e., energy donors with wide bandgap and large exciton diffusion length are introduced as sensitizers; (iii) excitons in the wide-gap antenna layers enter p- or n-type layers via efficient energy transfer, and then diffuse to and dissociate at the p–n junction; and (iv) efficient charge transport and collection of photogenerated charge carriers can be realized if no significant barriers for holes and/or electrons from the p–n junctions to the energy donors/antenna layers exist.

Using this concept for the purpose of improving photon harvesting in OSC, Hong et al. [149] combined two hole-conducting materials, pentacene and ZnPC, and electron conducting C_{60} to construct three-component heterojunctions. Figure 25c shows the absorption spectra of the three active materials and their molecular structures. Pentacene and ZnPC have strong absorption mainly in the longer wavelength range (500–800 nm). In pentacene/ZnPC/ C_{60} multi-heterojunction cells (see scheme in Fig. 25b), some of the excitons in pentacene might reach the ZnPC/ C_{60} interface, where efficient exciton separation occurs and contributes to the photocurrent. The V_{OC} of this device was slightly higher than that of the ZnPC/ C_{60} cell, which suggests a higher carrier concentration under the same illumination density, due to sensitization effects of pentacene for the ZnPC interlayer.

PC and PP [150–153] have also been added to polymer/fullerene systems to improve light-harvesting. For example, solar cells with multilayer structure containing P3HT, PCBM, and CuPC have been reported (Fig. 26) [151]. In these devices, the CuPC layer was thermally evaporated onto the substrate and the P3HT:PCBM layer was deposited by spin-coating. For solar cells with optimized layer thicknesses, enhanced light absorption was responsible for the high J_{SC} (12.5 mA cm^{-2}) and high efficiency (4.1%), a consequence of a second optical interference peak in the multilayer structure.

Cyanoporphyrins have also been incorporated into the active layer of P3HT:PCBM solar cells, which were obtained by spin-casting the blends from chloroform solutions [154]. Before annealing, the greatest PP contribution to the spectral response occurred when both P3HT and PCBM were present. Upon

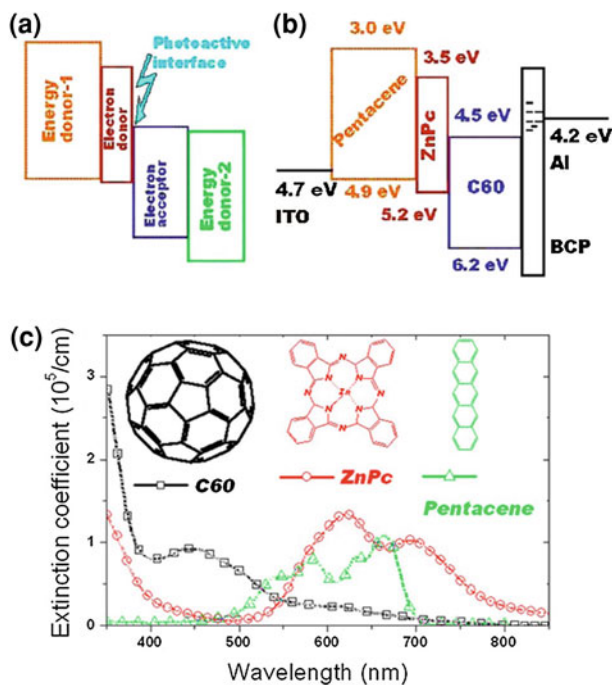


Fig. 25 **a** Concept of multiple-heterojunction design. **b** Energy diagram of OSC based on pentacene/ZnPc/C₆₀ multiple heterojunctions. **c** Extinction coefficient curves of the three materials and their molecular structures. “Reprinted with permission from Hong et al. [149]. Copyright [2009], American Institute of Physics”

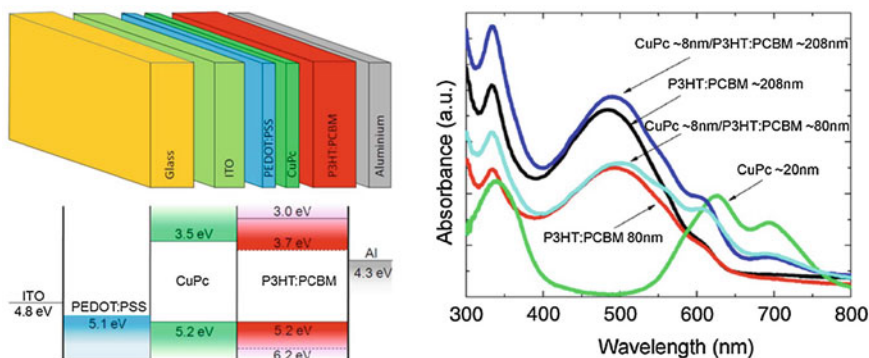


Fig. 26 Schematic illustration of the device structure and energy diagram for an OSC of ITO/PEDOT:PSS/CuPC/P3HT:PCBM/Al. The absorption spectra of P3HT:PCBM (80 nm), P3HT:PCBM (208 nm), CuPC (20 nm), CuPC (8 nm)/P3HT:PCBM (80 nm), and CuPC (8 nm)/P3HT:PCBM (208 nm) structures. “Reprinted with permission from Zhang et al. [151]. Copyright [2008], American Institute of Physics”

annealing (140°C for 4 min), the photocurrent generated by the PP was lost, due to aggregation, except in devices where only a small amount of polymer was present. For devices with low PCBM content, the PP did not contribute to the photocurrent and hindered the photocurrent generation by P3HT at the Soret band. Overall, this data suggests that the PP tends to interact with the polymer to quench photocurrent generation, but interacts preferentially with PCBM when it is present in the film.

In order to improve the exciton diffusion length, both high-mobility compounds and triplet materials with long exciton lifetimes can be introduced in the device. An efficient bulk-heterojunction OSC based on the triplet material 2,3,7,8,12,13,17,18-octaethyl-21*H*,23*H*porphineplatinum (II) was demonstrated by Shao and Yang [155]. Schulz and Holdcroft [156] and Yang et al. [157] also showed enhanced photovoltaic responses due to singlet-to-triplet exciton conversion in conjugated polymer/iridium complex-based cells. Li et al. [158] fabricated ITO/PEDOT:PSS/P3HT:Pt dendrimer/C₆₀/Al cells, in which the charge generating structure consisted of a film of P3HT blended with triplet platinum dendrimer complex deposited by spin-coating and a thermally evaporated fullerene layer. In this platinum dendrimer, the platinum porphyrin core acts as heavy metal center, which induces intersystem crossing in the host polymer [157, 159], and the external carbazole groups enhance the conductive properties. In particular, the alkyl chains provide good solubility for the dendrimers in organic solvents and excellent film-forming properties by spin-coating. The cells showed a poor efficiency of 0.70%, which was attributed to poor mobility in the Pt dendrimer film.

The construction of supramolecular assemblies is also interesting and promising for the future development of photovoltaics. In this perspective, recent developments of supramolecular systems for light energy conversion, which are mainly composed of PC dyes and nanocarbon materials, such as fullerenes and carbon nanotubes were reported. The water-soluble CuPC derivative 3,4,4,4 tetrasulphonic acid tetra sodium salt copper phthalocyanine (TS-CuPC) was blended with concentrated dispersions of acid-treated carbon nanotubes to form stable solutions with excellent film-forming properties [160]. The application of this nanocomposite material as hole-extracting electrode and donor layer in bilayer OSC using C₆₀ as electron acceptor was demonstrated. The interaction between surface-oxidized multi-walled carbon nanotubes (o-MWCNTs) and TS-CuPC was also investigated [161]. The compatibility between the two components was shown to result from hydrogen-bonding interactions and ground-state charge-transfer interactions. The self-organization of the o-MWCNT decorated PC molecules into extended aggregates of 1D linearly stacked PC polymers was observed to occur after the spin-coating deposition. The hybrid material was incorporated into an organic photovoltaic cell at the interface between the P3HT:PCBM bulk-heterojunction layer and the ITO electrode. This extra-layer increased the light-harvesting and facilitated the hole extraction, enhancing the η .

Despite the interesting concepts underlying the introduction of a third component to the OSC, more efforts are necessary in the search for better material combinations, since higher efficiencies are still found for two-component-based devices.

6 Small Molecules in Dye-sensitized Solar Cells

The possibility of exploring the solar energy with reduced costs became a reality after the report of an efficient DSSC by O'Regan and Grätzel [162]. Since then these devices have attracted significant attention from the scientific and industrial community because DSSCs use cheaper materials and production processes than the analogous Si-based photovoltaics. These solar cells can achieve up to 10.4% of certified solar power efficiency [163] and their stability data indicates at least 10 years of use in outdoor applications [164]. Generally, DSSCs are assembled using nanocrystalline TiO₂, organic or inorganic dyes (normally Ruthenium (II) coordination compounds), and a liquid electrolyte. The liquid component is considered a drawback for large-area production as a consequence of potential liquid leakage and contamination concerns; a sealed and secured cell is essential. Also, the iodine usually employed is capable of attacking the transparent conducting oxide substrate typically used in fabrication. Solid or quasi-solid electrolytes, such as polymers and gels, have been applied as alternatives to the liquid component [165–167]. However, all-solid-state solar cells are only achievable when p-type semiconductors are employed, such as inorganic hole conductors, organic low-molecular weight molecules or conducting polymers [168–173, 218–220].

In this scenario, small organic molecules are also promising candidates to replace the liquid electrolyte for several reasons: easy fabrication, low cost, and versatile deposition. When applied as hole conductors (or hole transporting materials, HTM) in DSSCs, better penetration is achieved due to their ability to fill the TiO₂ pores more effectively.

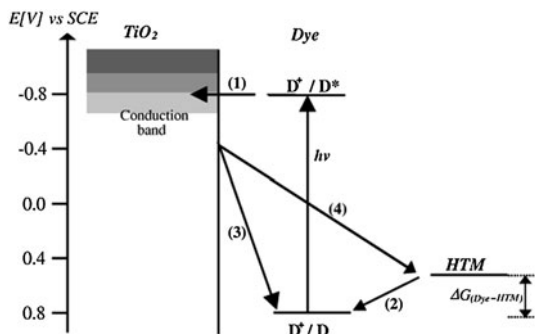
Small organic molecules can also be used to replace the sensitizer dye in DSSCs. In fact, in recent years, several groups have concentrated their efforts in the search of novel organic dyes with more extended light absorption toward the infrared. Besides, the small organic dye can replace the expensive metal complexes based on the rare metal Ruthenium [174–176]. It is also possible that the sensitizer dye acts simultaneously as both absorber and HTM in this kind of solar cell, although the efficiency is low.

In this section we will focus mainly on the attempts to replace the liquid electrolyte in DSSC by small organic molecules as HTMs. Small molecules are powerful sensitizers, particularly perylene, indoline and arylamine derivatives. Due to the great versatility and performance demonstrated in DSSC, a brief review is provided for this application.

6.1 Hole-Conductor Materials

Energy conversion in a DSSC is based on the injection of an electron from a photoexcited state of the sensitizer dye (typically a bipyridine Ruthenium (II) complex) into the conduction band of the nanocrystalline semiconductor (TiO₂ is

Fig. 27 Schematic diagram of the processes occurring at the dye-sensitized TiO_2 /organic HTM heterojunction (Haque et al. [217]). Copyright Wiley-VCH Verlag GmbH & Co. KGaA. Reproduced with permission



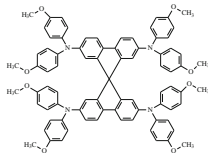
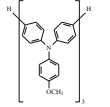
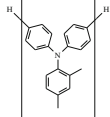
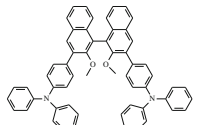
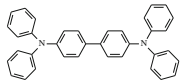
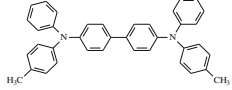
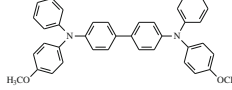
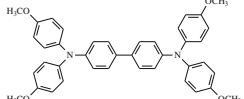
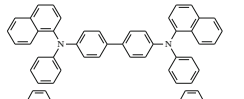
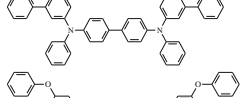
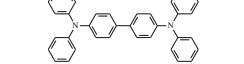
by far the most employed oxide semiconductor), as depicted in Fig. 27. These cells also employ a liquid electrolyte (usually an iodide/triiodide redox-active couple dissolved in an organic solvent) to reduce the dye cation (viz., regenerate the ground state of the dye). Regeneration of iodide ions, which are oxidized in this reaction to triiodide, is achieved at a platinum counter electrode.

A p-type semiconductor can replace the liquid electrolyte if it is able to accept holes efficiently from the excited state of the dye cation. The main processes that occur at the TiO_2 /dye/HTM interfaces are represented in Fig. 27. Cell operation using HTM is analogous to liquid or polymer electrolyte-based DSSCs. However, after dye excitation and electron transfer (reaction 1 in Fig. 27), the ground state of the dye is regenerated by the HTM (reaction 2): electrons from the HOMO of the HTM regenerate the ground state of the dye molecules instead of the redox couple of the electrolyte. The oxidized HTM material is then reduced at the counter electrode (in most cases a nanometric layer of gold). The main difference relies on the kind of transport between the electrodes. In comparison to the ionic transport in the DSSC which uses liquid or gel polymer electrolyte, the HTM cell transport is typically electronic. The losses are represented by the electron recombination with the dye cations (reaction 3) and with HTM (reaction 4). The recombination reactions are important because they limit the efficiency of these solar cells: at open-circuit and short-circuit conditions, the recombination is 10 and 100 times faster than in the cells with liquid electrolyte, respectively [177].

The hole-transfer reaction is limited by the thermodynamic driving force, defined as $\Delta G_{\text{dye-HTM}}$ [169]. In order to achieve an 85% charge-transfer yield, the energy difference between the HOMO of the HTM and the HOMO of the dye ($\Delta G_{\text{dye-HTM}}$) must be at least 0.2 eV. According to the energy diagram, the HOMO position of the HTM must lie above the ground state of the sensitizer dye.

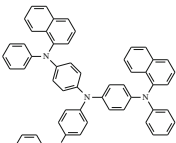
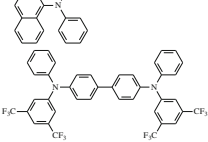
Triarylamine derivatives are so far the most important class of HTM applied in DSSC. The first successful triarylamine derivative applied in DSSC was the amorphous compound 2,2',7,7'-tetrakis-(*N,N*-di-*p*-methoxyphenylamine)9,9'-spirobifluorene (referred as spiro-OMeTAD, structure 1, Table 3), introduced by the group of Prof. M. Grätzel in 1998 [168]. In 2007, the efficiency of the solid-state DSSC based on spiro-OMeTAD reached 5.1% [178]. Until this present day, this molecule has been unsurpassed in terms of hole conduction in DSSC. However,

Table 3 Characteristics of some organic HTM based on triarylamine derivatives applied in DSSCs

Structure	Mw	Hole mobility/ $\text{cm}^2 \text{V}^{-1} \text{s}^{-1}$	HOMO level/ eV	References
1 	1230	2×10^{-4} (a)	-4.77	[170]
2 	821	4.86×10^{-4} (b)	-4.97	[169]
3 	815	8.07×10^{-4} (b)	-5.0	[169]
4 	800	(c)	-5.26	[171]
5 	488	10^{-3} (a)	(c)	[172, 173]
6 	516	$\sim 10^{-3}$ (a)	-5.13	[172, 173]
7 	548	$\sim 10^{-3}$ (a)	-5.06	[172, 173]
8 	608	$\sim 10^{-3}$ (a)	-4.97	[173]
9 	588	$\sim 10^{-3}$ (a)	-5.20	[173]
10 	688	$\sim 10^{-3}$ (a)	-5.18	[173]
11 	640	$\sim 10^{-3}$ (a)	-5.12	[173]

(continued)

Table 3 (Continued)

Structure	Mw	Hole mobility/ $\text{cm}^2 \text{V}^{-1} \text{s}^{-1}$	HOMO level/ eV	References
12 	896	(^c)	(^c)	[173]
13 	760	(^c)	-5.45	[173]

^a Determined using the time-of-flight technique

^b Field-effect transistor (FET) mobilities

^c Not available

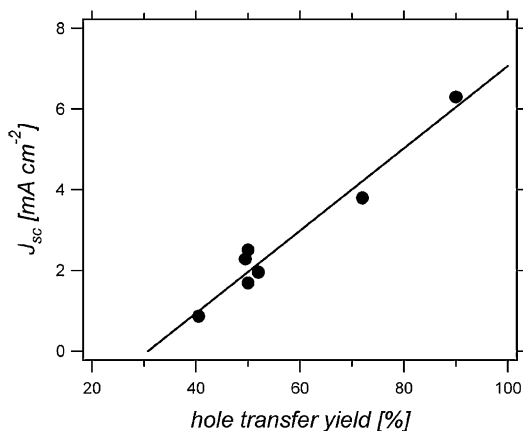
other types of organic HTMs have been synthesized and have demonstrated the potential to replace liquid electrolytes, as well. Table 3 summarizes the structures and some characteristics of small organic HTM based on triarylamine derivatives applied in DSSC.

Interestingly, the charge-transport properties of the spiro-OMeTAD showed that its hole mobility is independent of film thickness from 0.135 to 4 μm [170]. Thus, hole mobility is a non-dispersive characteristic and this indicates that the photocurrent may be dependent on the rate of interfacial hole transfer, not as function of the thickness. In fact, Durrant et al. [169] found that the hole transfer yield (related to the efficiency of reaction 2 presented in Fig. 27) is directly proportional to the photocurrent (Fig. 28).

Although a high hole mobility is a strong consideration when choosing between potential HTMs, other important requirements must be taken into. It is well-established that good film-formation ability, low tendency toward crystallization, and excellent pore filling and HOMO energy value strongly influence the overall conversion efficiency of DSSCs [173]. As observed in the performance of solar cells using the hole conductors 1–3 as displayed in Table 3, the best efficiency was achieved with spiro-OMeTAD (2.8%), although this molecule presented the lowest hole mobility of all. Despite the higher hole mobility of the other triarylamine oligomers, they are poor pore fillers [179] and have significant variations in the hole transfer yields.

Similar conclusions involving the HTM properties and their relation to device performance were obtained out by Karthikeyan and Thelakkat using several synthesized HTMs based on triphenyldiamines with mobility of the order of $10^{-3} \text{cm}^2 \text{V}^{-1} \text{s}^{-1}$ [173]. They calculated the charge-transfer rate for these molecules and observed their dependence on the HOMO energy offset. The maximum charge-transfer rate was realized for the energy gap of 0.79 eV. The results give significant information for the design of novel dyes and HTM.

Fig. 28 Short-circuit photocurrent density (J_{SC}) as a function of the hole transfer yield, determined using Transient Absorption Spectroscopy—TAS (Kroeze et al. [169]). Copyright Wiley–VCH Verlag GmbH & Co. KGaA. Reproduced with permission



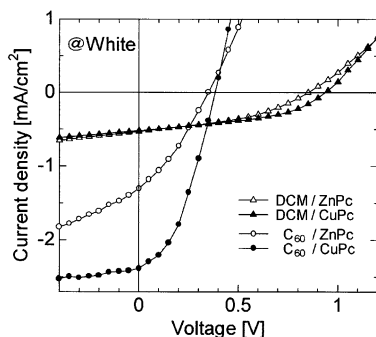
Another class of HTM is macrocyclic aromatic compounds such as PP and PC. They have high stability and high optical absorption, covering a great extension of the solar spectrum. Some techniques have showed that PP and PC films are frequently p-type semiconductors [180–184]. Few reports demonstrate the usage of this class of small molecules in transporting holes after dye excitation. The combination of TiO_2 and PC or PP is limited [185–190], and the efficiency is low. For the $\text{TiO}_2/\text{ZnPC}/\text{Au}$ cells, $V_{OC} = 0.376$ V, $J_{SC} = 0.142$ mA cm^{-2} , and $FF = 0.34$ (under simulated AM 2 conditions) were achieved [185]. Other reports were found for zinc (ZnPC) [185, 189, 190], copper (CuPC) [190], palladium (PdPC) [185], lead (PbPC) [188], and iron (II) phthalocyanines (FePC) [187]. The best result was obtained for an $\text{ITO}/\text{TiO}_2/\text{ZnTCPP}/\text{Hg}$ solar cell (where ZnTCPP is zinc-tetra(4-carboxyphenyl) porphyrin), which showed a V_{OC} of 0.7 V, J_{SC} of 0.22 mA cm^{-2} , and FF of 0.25 [182].

For the most part, these molecules, PP and PC are more intensively explored as dyes [191–198]. The dual function of this class of small molecules, as sensitizer and as HTM, is rarely investigated [182]. A possible explanation for the limited use of PP and PC as HTMs (and dye-HTM combination) in DSSCs comes from low efficiency and this may be related to the difficulty of filling the pores of the TiO_2 electrodes, annihilation of the molecule excited state by energy transfer due to aggregation, and poor hole mobility after deposition. In fact, for this class of molecules, the values of hole mobility is closely related to device performance.

Intensity-modulated photocurrent spectroscopy indicates that the transport of holes in these small molecules is not governed by the electric field, but driven by diffusion [182]. Mobility values of 5 and 2.5×10^{-4} $\text{cm}^2 \text{V}^{-1} \text{s}^{-1}$ were found for columnar stacks of PP [199] and a palladium phthalocyanine (PdPC) [186]. In this latter case the solar cell presented a $V_{OC} = 0.46$, $J_{SC} = 30$ $\mu\text{A cm}^{-2}$, $FF = 0.35$ and $\eta = 0.025\%$ under 20 mW cm^{-2} . However, in the majority reports, the mobility values fall between 10^{-10} and 10^{-7} $\text{cm}^2 \text{V}^{-1} \text{s}^{-1}$ [181, 182].

It is also important, however, to call attention to the difficulty in preparing such films. This may explain the large discrepancy between the reported mobilities

Fig. 29 I–V curves of DCM and C₆₀ based devices as an intermediate layer, which is sandwiched between TiO₂ and ZnPC or CuPC layer under white light illumination. “Reprinted from Ohmori et al. [190], copyright (2006), with permission from Elsevier”



values derived from current–voltage [200, 201], time-of-flight [202] and microwave-conductivity measurements [199], since only vacuum sublimation, electropolymerization and dispersion in other HTMs seems to be a successful method to achieve homogeneous and stable films [183].

Nevertheless, the conversion efficiency can be substantially increased when dyes or electron acceptors such as C₆₀ and 4-(dicyano-methylene)-2-methyl-6-(4-dimethylaminostyryl)-4H-pyran (DCM) are added as n-type material in ITO/TiO₂/n-type layer/PC/Au cells, where PC refers to ZnPC or CuPC [190]. The hole mobilities were estimated as 3.8×10^{-3} and $2.6 \times 10^{-5} \text{ cm}^2 \text{ V}^{-1} \text{ s}^{-1}$ for CuPC and ZnPC, respectively. The largest energy difference between the HOMO level of PC and LUMO level of DCM leads to an increase in the V_{OC} of the device. The best solar cell performance was achieved with C₆₀ combined with CuPC (Fig. 29), which causes an increase of J_{SC} , likely due to a higher carrier mobility, i.e., C₆₀ acts as an electron acceptor, increasing the electron transport.

Pentacene molecules have also been applied as HTM in DSSC, however, the efficiency of the solar cells is lower compared with triarylamine derivatives, possibly due to a fast recombination of the charge carriers at the interfaces [203].

6.2 Small Molecules as Sensitizers

In DSSCs, the photocurrent values are limited by the absorption spectrum of the sensitizer dye. Tuning the optical and electronic properties of small organic molecules by modifying their chemical structures has become an important step in overcoming this issue and developing solar cells with improved light-harvesting capabilities. In fact, the number of publications involving the synthesis of novel organic dyes and their application as sensitizers in DSSCs has grown rapidly, motivated by the high efficiency values reported recently (Fig. 30). The best result achieved to date reached 9.8% of efficiency using a TPA derivative and a liquid electrolyte [204].

Among the organic molecules sensitizers, cyanine [174], coumarin [205], porphyrins [191–194], phthalocyanine [192, 195–198], perylene derivatives [206–209],

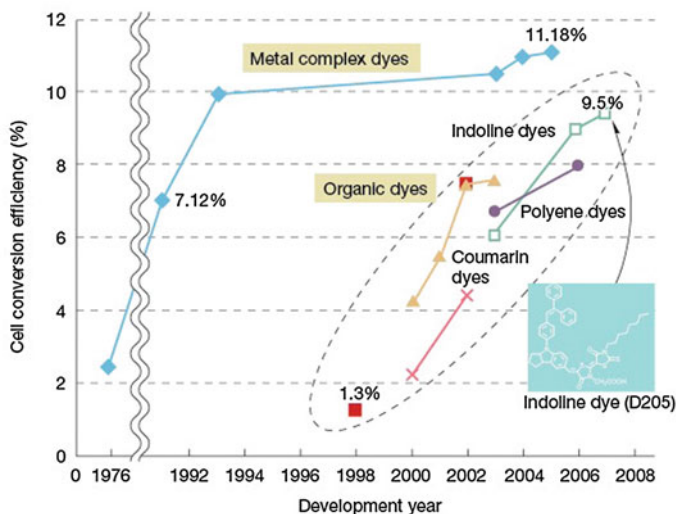


Fig. 30 Ruthenium complexes developed by the Grätzel Group in 1991 achieved an efficiency of 10% quite rapidly and they are currently at 11%. The use of organic dyes began with extremely low efficiencies but has shown a fast growth in the last years. The D205 developed by Mitsubishi Paper Mills in 2007 achieves an efficiency of 9.5% (from Tetsuo Nozawa Nikkei Electronics Asia, July 2008) (<http://www.sciencedirect.com/science/journal/00406090>)

indoline [175, 176] and arylamine derivatives dyes [204, 210, 211] have received particular attention. In this section we will focus on perylene, indoline, and arylamine dyes, since recent reviews on the use of cyanine [174], coumarin [174], porphyrin [192, 193], and phthalocyanine [192] dyes in solar cells can be found elsewhere. The perylene derivatives present high stability and high versatility attained by use of different functional groups. Indoline/arylamine dyes have shown the highest efficiency for organic dyes in DSSCs [176, 204].

Photophysical studies are a powerful tool to monitor the excited state of these molecules and to correlate the effect of the substituent groups in molecular dynamics. For example, the degree of dye aggregation can be modulated by substituents like alkyl side-chains with free rotation capacities. Long alkyl chains [206] and 2,6-diisopropylphenyl [207] have demonstrated promising results and are shown in Fig. 31.

The presence of two alkyl chains in perylene (Fig. 31) showed that a free rotation capacity prevents aggregation, enhancing the photoelectron transfer injection from the dye to the titania film. Icli et al. [206] showed that the presence of two chains instead of one long or small chains with many substituents prevents charge recombination, resulting in photocurrent values up to 9 mA cm^{-2} and an efficiency of 1.61%. When the substituent group is larger and possesses strong electron-donating properties (i.e., two pyrrolidines at the perylene core) as in perylene b (Fig. 31), the first oxidation potential is shifted in the negative direction, improving the power-conversion efficiency up to 2% [207].

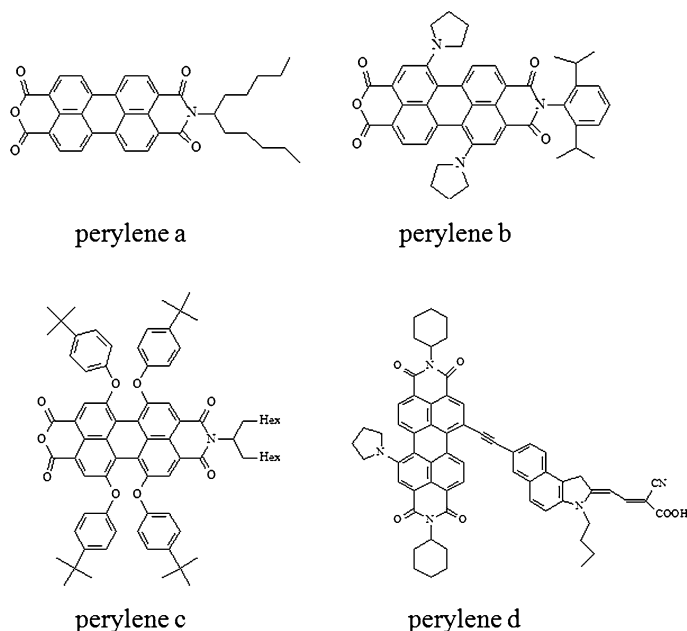
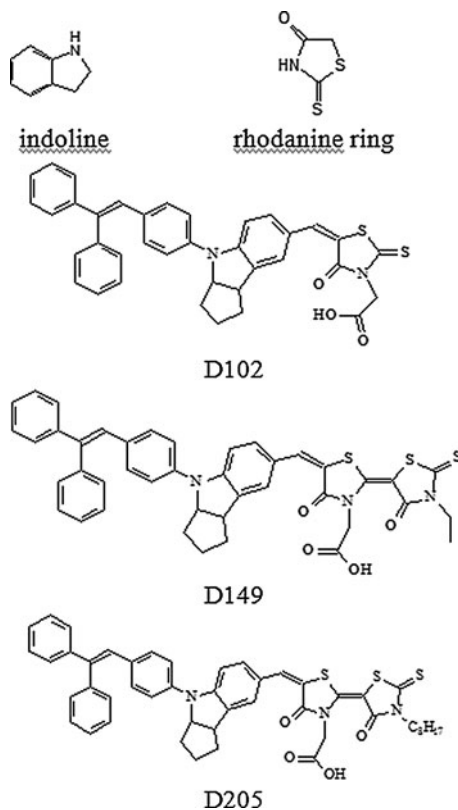


Fig. 31 Structures of perylene derivatives [206–209]

In addition, the presence of four O-aryl groups makes the perylene sufficiently electron donating when applied as TiO_2 sensitizer. The conjugation system between the perylene core and the benzimidazole was tested and leads to a significant bathochromic shift of the absorption maximum and to an enhanced molar absorption coefficient. However, the electron injection was low, with efficiencies below 1%. The absence of benzimidazole and the presence of alkyl chain (perylene c, Fig. 31) led to a decrease in the dye recombination, reaching an efficiency of 2.29% [208]. An interesting report by Jin et al., demonstrated that the presence of two imide groups (perylene d, Fig. 31) in a perylene dye deteriorated device performance. Such molecules contain a strong electron-withdrawing group, resulting in ineffective electron transfer to the carboxylic groups anchored on the TiO_2 [209].

Other organic dyes have also shown promise in the DSSC field. Indoline dyes are a class of molecules with high sensitization. The presence of a rhodanine ring in the indoline dyes (Fig. 32) contributed to a red shift in the absorption spectrum, resulting in devices with a $V_{\text{OC}} = 693$ mV, $J_{\text{SC}} = 18.50$ mA cm^{-2} , $\text{FF} = 0.624$, and $\eta = 8.00\%$ [175]. Solid-state DSSCs using spiro-OMeTAD and D102 dye have been reported. The devices showed efficiency higher than 4% [212]. The introduction of a *n*-octyl substituent onto the rhodanine ring (D205 in Fig. 32) has pushed the conversion efficiency up to 9.52% under 100 mW cm^{-2} . This is the highest value reported so far for an indoline dye-based DSSC, compared to the same cells using Ruthenium (II) complexes [175].

Fig. 32 Molecular structures of indoline, rhodanine ring, and indoline dyes D102, D149, D205 [175, 176, 213]



The high efficiency values can be explained by a red shift caused by attaching a second rhodanine unit to the indoline structure, extending its π -conjugation [213]. Although the chromophoric units of these two dyes are identical and the IPCEs are very close [175], the best behavior of D205 (Fig. 33) is a result of the extension of the alkyl chain on the terminal rhodanine moiety from ethyl to octyl. The successful combination of the *n*-octyl chain in the dye with the adsorption cheno-deoxycholic acid (CDCA) onto the oxide resulted in blocking the charge recombination between I_3^- and electrons injected in the nanocrystalline-TiO₂ electrodes [176].

However, the D205 indoline does not seem to be stable for use in outdoor photovoltaic devices [214]. Thus, arylamine derivatives dyes have been synthesized to improve the resistance to degradation over light soaking at full solar intensity and elevated temperatures [204, 215, 216]. These dyes contain an arylamine (electron donor) and a cyanoacrylate group (electron acceptor) connected by one or several thiophene moieties acting as a π -conducting bridge. During light excitation, electrons are transferred from the arylamine through the thiophene bridge to the surface-bound cyanoacrylate, producing an efficient and rapid electron injection from the excited state of the sensitizer into the conduction band of the TiO₂ [214].

Fig. 33 Current density vs. voltage characteristics for DSSC with indoline dyes (D149 and 205) as sensitizers with/without chenodeoxycholic acid (CDCA) under AM1.5 simulated sunlight (100 mW cm^{-2}) illumination. Ito et al. [176]—reproduced by permission of The Royal Society of Chemistry

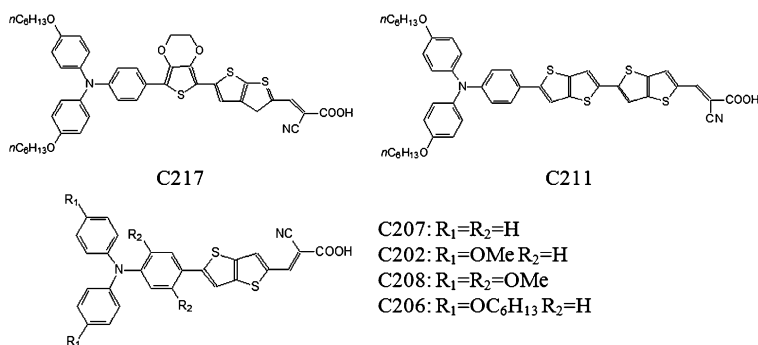
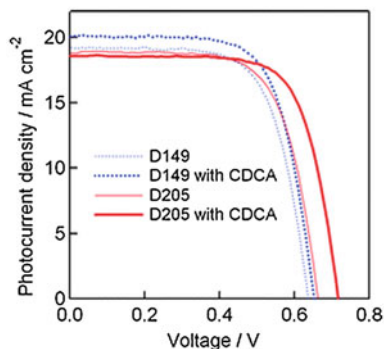


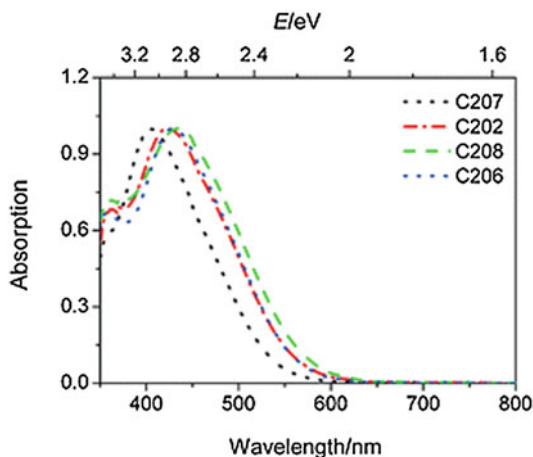
Fig. 34 Structures of the arylamine derivatives dyes [204, 210, 211] (<http://dx.doi.org/10.1039/B809093A>)

Due to the strong coupling of the excited state wave function with the Ti ($3d, t_{2g}$) orbitals [214], the record efficiency of 9.8% is reached using organic dyes that belongs to an arylamine derivative dye named C217, shown in Fig. 34. Such a remarkable dye combines an electron donor and an electron acceptor with an electron-rich 3,4-ethylenedioxythiophene unit that has a small torsion angle with respect to the adjoining phenyl fragment, ensuring efficient electronic communication between donor and acceptor units [204].

An analogous thiophene π -conducting bridge (thienothiophene and bithienothiophene) has also been demonstrated (C207, C202, C208, C206 e C211 in Fig. 34) [210, 211], showing that the addition of one more thienothiophene units both increases HOMO level slightly and drives down the LUMO, narrowing the gap [210]. Comparing the dyes in Fig. 35, the band gap can be further shifted into the infrared regime when two electron-donating methoxy groups (C208) are replaced at R_1 positions [211].

Although DSSCs employing indolines and arylamines have demonstrated improved and impressive results in recent years, the overall power-conversion efficiencies still remain slightly below the values achieved with expensive

Fig. 35 Normalized absorption spectra of C207, C202, C208 and C206 dyes anchored the nanocrystalline titania film. The absorption from the titania and glass substrate has been subtracted. "Reprinted with permission from Xu et al. [211]. Copyright 2008 American Chemical Society"



ruthenium complexes. However, scientists working in this field foresee that the most powerful solar cells will be those based on organic dyes. Theoretical chemical calculation, for example, is a powerful tool that can help us design and select new dyes with more suitable absorption spectra, and as consequence, increased light-harvesting abilities.

7 Conclusions and Perspectives

Any emerging technology represents a challenging task and this is no different in the development of efficient, stable OSCs based on small molecules. This field requires a multidisciplinary contribution that involves strong cooperation between creative synthetic chemists, solid-state physicists, theoreticians, and device engineers.

The efficiency of OSCs based on small molecules is currently inferior to those employing conjugated polymers. This is partially attributed to the contact interfaces. A polymer adsorbed on a surface can only desorb if a substantial number of its segments desorb simultaneously, which is improbable and slow. However, interface quality and stability in small molecule devices have been lacking. Thus, more stable interfaces are required.

In addition to searching for novel donor and acceptor molecules with improved solubility, light-harvesting capability and charge mobility, the most challenging and critical issue is to achieve a suitable morphology without phase separation in solution-processed OSCs. It is very common to find FF values below 50% in solar cells using the solution approach. Tryarilamines, vinazene, and diketopyrrolopyrrol-based molecules are among the most promising candidates for solution processable solar cells. In the case of vinazene molecules, values of open-circuit voltage exceeding 1 V were obtained. Efficiency is expected to increase with

better control over phase separation and the use of self-assembly techniques may be interesting in this context.

Solar cells based on evaporated small molecules offer an alternative to SPOSCs as OS films and/or multilayers can be easily deposited with high purity, high crystallinity, and without pinholes. VTE and OVPD are the most-used techniques, providing morphological control in the double layer, bulk heterojunction and tandem approaches. The introduction of an EBL has allowed efficiencies up to 4%. Besides those advantages, the major drawback is the cost associated with the production method, especially for large-area solar cells.

Organic small molecules have also found their place as components in hybrid solar cells, which include dye-sensitized solar cells. In this type of device, organic molecules can act as both the dye and hole transporting materials. In fact, the field of DSSCs has grown intensively in the area of novel small organic molecules with ability to absorb long wavelengths. The indoline dyes represent the DSSC-ruthenium free class that has delivered the highest efficiencies to date.

As HTMs, triarylamine derivatives, especially Spiro-OMeTAD, are the most studied class of p-type semiconductors. The replacement of the liquid electrolyte by an HTM is not trivial. Problems associated with poor electrode filling, HOMO position (which controls the charge transfer yield) and mobility still need to be solved.

For OSCs in general, the challenges are many. As solar cell efficiencies improve, however, long-term device stability becomes a more relevant and important issue to consider. Novel donor and acceptor molecules with improved optical, electronic, and transport properties are desired. Control over morphology is experimentally difficult and efforts in this direction continue to receive increasing attention. Although most OSCs employ amorphous films, partly because it is relatively easy to deposit amorphous pinhole-free films that adhere well to substrates and to other films, a tendency to produce more crystalline and/or aligned OSs has been observed. New cell architectures, the design of an appropriate DA combination based on theoretical investigations, more ordered structures and stable interfaces have been pointed out as strategies to push the efficiency of these solar cells toward a competitive level. The future is bright for OSCs and based on recent achievements there is no doubt that their place is certainly guaranteed in the photovoltaic market.

Acknowledgments The authors thank CNPq, Fapesp (2009/15428-0, 2008/53059-4) and INEO (National Institute for Organic Electronics) for financial support and scholarships. The authors also acknowledge Jason Guy Taylor and Prof. Roy Bruns for English revision.

References

1. Nelson J (2004) *The physics of solar cells*. Imperial College Press, London
2. Brabec CJ, Dyakonov V, Parisi J, Sariciftci NS (2003) *Organic photovoltaics: concepts and realization*. Springer, Berlin

3. Sun S-S, Sariciftci NS (2005) *Organic photovoltaics*. Taylor & Francis Group, Boca Raton
4. Würfel P (2009) *Physics of solar cells*. Wiley-VCH, Weinheim
5. Archer MD, Hill R (2005) *Clean electricity from photovoltaics*. Imperial College Press, London
6. Archer MD, Nozik AJ (2008) *Nanostructured and photoelectrochemical systems for solar photon conversion*. Imperial College Press, London
7. Brabec C, Dyakonov V, Scherf U (2009) *Organic photovoltaics*. Wiley-VCH, Weinheim
8. Li JL, Dierschke F, Wu JS, Grimsdale AC, Mullen K (2006) Poly(2, 7-carbazole) and perylene tetracarboxydiimide: a promising donor/acceptor pair for polymer solar cells. *J Mater Chem* 16:96–100
9. Sharma GD, Suresh P, Mikroyannidis JA, Stylianakis MM (2010) Efficient bulk heterojunction devices based on phenylenevinylene small molecule and perylene-pyrene bisimide. *J Mater Chem* 20:561–567
10. Silvestri F, Irwin MD, Beverina L, Facchetti A, Pagani GA, Marks TJ (2008) Efficient squaraine-based solution processable bulk-heterojunction solar cells. *J Am Chem Soc* 130:17640–17641
11. Balakrishnan K, Datar A, Baddo T, Huang J, Otiker R, Yen M, Zhao J, Zang L (2006) Effect of side-chain substituents on self-assembly of perylene diimide molecules: morphology control. *J Am Chem Soc* 128:7390–7398
12. Winzenberg KN, Kempin P, Fanchini G, Bown M, Collins GE, Forsyth GM, Hegedus K, Singh TB, Watkins SE (2009) Dibenzo[b, def]chrysene derivatives: solution-processable small molecules that deliver high power-conversion efficiencies in bulk heterojunction solar cells. *Chem Mater* 21:5701–5703
13. Lloyd MT, Mayer AC, Subramanian S, Mourney DA, Herman DJ, Bapat AV, Anthony JE, Malliaras GGJ (2007) Efficient solution-processed photovoltaic cells based on an anthradithiophene/fullerene blend. *J Am Chem Soc* 129:9144–9149
14. Kronenberg NM, Deppisch M, Würthner F, Lademann HWA, Deing K, Meerholz K (2008) Bulk heterojunction organic solar cells based on merocyanine colorants. *Chem Commun* 6489–6491
15. Ma C-Q, Fonrodona M, Schikora MC, Wienk MM, Janssen RAJ, Bauerle P (2008) Solution-processed bulk-heterojunction solar cells based on monodisperse dendritic oligothiophenes. *Adv Funct Mater* 18:3323–3331
16. Velusamy M, Huang J-H, Hsu Y-C, Chou H-H, Ho K-C, Wu P-L, Chang W-H, Lin JT, Chu C-W (2009) Dibenzo[f, h]thieno[3, 4-b] quinoxaline-based small molecules for efficient bulk-heterojunction solar cells. *Org Lett* 11:4898–4901
17. Shirota Y (2000) Organic materials for electronic and optoelectronic devices. *J Mater Chem* 10:1–25
18. Shirota Y, Kageyama H (2007) Charge carrier transporting molecular materials and their applications in devices. *Chem Rev* 107:953–1010
19. Roncali J (1997) Synthetic principles for bandgap control in linear pi-conjugated systems. *Chem Rev* 97:173–205
20. Roncali J (2005) Linear-conjugated systems derivatized with C60-fullerene as molecular heterojunctions for organic photovoltaics. *Chem Soc Rev* 34:483–495
21. He C, He Q, Yi Y, Wu G, Bai F, Shuai Z, Li Y (2008) Improving the efficiency of processable organic photovoltaic devices by a star-shaped molecular geometry. *J Mater Chem* 18:4085–4090
22. Zhang J, Yang Y, He C, He Y, Zhao G, Li Y (2009) Solution-processable star-shaped photovoltaic organic molecule with triphenylamine core and benzothiadiazole-thiophene arms. *Macromolecules* 42:7619–7622
23. Wu G, Zhao G, He C, Zhang J, He Q, Chen X, Li Y (2009) Synthesis and photovoltaic properties of a star-shaped molecule with triphenylamine as core and benzo[1, 2, 5]thiadiazol vinylene as arms. *Sol Energy Mater Sol Cells* 93:108–113

24. Li W, Du C, Li F, Zhou Y, Fahlman M, Bo Z, Zhang F (2009) Benzothiadiazole-based linear and star molecules: design, synthesis, and their application in bulk heterojunction organic solar cells. *Chem Mater* 21:5327–5334
25. Li K, Qu J, Xu B, Zhou Y, Liu L, Peng P, Tian W (2009) Synthesis and photovoltaic properties of a novel solution-processable triphenylamine-based dendrimers with sulfonyldibenzene cores. *New J Chem* 33:2120–2127
26. He C, He Q, Yang X, Wu G, Yang C, Bai F, Shuai Z, Wang L, Li Y (2007) Synthesis and photovoltaic properties of a solution-processable organic molecule containing triphenylamine and DCM moieties. *J Phys Chem C* 111:8661–8666
27. Xue L, He J, Gu X, Yang Z, Xu B, Tian W (2009) Efficient bulk-heterojunction solar cells based on a symmetrical D–A–D organic dye molecule. *J Phys Chem C* 113:12911–12917
28. Zhao G, Wu G, He C, Bai F-Q, Xi H, Zhang H-X, Li Y (2009) Solution-processable multiarmed organic molecules containing triphenylamine and DCM moieties: synthesis and photovoltaic properties. *J Phys Chem C* 113:2636–2642
29. Tang CW (1986) Two layer organic photovoltaic cell. *Appl Phys Lett* 48:183–185
30. Takahashi K, Asano M, Imoto K, Yamaguchi T, Komura T, Nakamura J, Murata K (2003) Sensitization effect of porphyrin dye on the photocurrent of Al/polythiophene schottky-barrier cells. *J Phys Chem B* 107:1646–1652
31. Takahashi K, Nakajima I, Imoto K, Yamaguchi T, Komura T, Murata K (2003) Sensitization effect by porphyrin in polythiophene/perylene dye two-layer solar cells. *Sol Energy Mater Sol Cells* 76:115–124
32. Peumans P, Forrest SR (2001) Very-high-efficiency double-heterostructure copper phthalocyanine/C-60 photovoltaic cells. *Appl Phys Lett* 79:126–128
33. Stübinger T, Brütting W (2001) Exciton diffusion and optical interference in organic donor-acceptor photovoltaic cells. *J Appl Phys* 90:3632–3641
34. Ma B, Woo CH, Miyamoto Y, Frechet JMJ (2009) Solution processing of a small molecule, subnaphthalocyanine, for efficient organic photovoltaic cells. *Chem Mater* 21:1413–1417
35. Matsuo Y, Sato Y, Niinomi T, Soga I, Tanaka H, Nakamura E (2009) Columnar structure in bulk heterojunction in solution-processable three-layered p–i–n organic photovoltaic devices using tetrabenzoporphyrin precursor and silylmethyl[60]fullerene. *J Am Chem Soc* 131:16048–16050
36. Huang X, Zhu C, Zhang S, Li W, Guo Y, Zhan X, Liu Y, Bo Z (2008) Porphyrin-dithienothiophene-conjugate copolymers: synthesis and their applications in field-effect transistors and solar cells. *Macromolecules* 41:6895–6902
37. Tamayo AB, Walker B, Nguyen TQ (2008) A low band gap, solution processable oligothiophene with a diketopyrrolopyrrole core for use in organic solar cells. *J Phys Chem C* 112:11545–11551
38. Tamayo AB, Dang XD, Walker B, Seo J, Kent T, Nguyen TQ (2009) A low band gap, solution processable oligothiophene with a dialkylated diketopyrrolopyrrole chromophore for use in bulk heterojunction solar cells. *Appl Phys Lett* 94:103301-1–103301-3
39. Walker B, Tamayo AB, Dang X-D et al (2009) Nanoscale phase separation and high photovoltaic efficiency in solution-processed, small-molecule bulk heterojunction solar cells. *Adv Funct Mater* 19:3063–3069
40. Tamayo A, Kent T, Tantitiwat M, Dante MA, Rogers J, Nguyen T-Q (2009) Influence of alkyl substituents and thermal annealing on the film morphology and performance of solution processed, diketopyrrolopyrrole-based bulk heterojunction solar cells. *Energy Environ Sci* 2:1180–1186
41. Rand BP, Li J, Xue J, Holmes RJ, Thompson ME, Forrest SR (2005) Organic double-heterostructure photovoltaic cells employing thick *tris*(acetylacetonato)ruthenium(III) exciton-blocking layers. *Adv Mater* 17:2714–2718
42. Li G, Shrotriya V, Huang J, Yao Y, Moriarty T, Emery K, Yang Y (2005) High-efficiency solution processable polymer photovoltaic cells by self-organization of polymer blends. *Nat Mater* 4:864–868

43. Peet J, Kim JY, Coates NE, Moses D, Heeger AJ, Bazan GC (2007) Efficiency enhancement in low-bandgap polymer solar cells by processing with alkane dithiols. *Nat Mater* 6:497–500
44. Goh C, Scully SR, McGehee MD (2007) Effects of molecular interface modification in hybrid organic–inorganic photovoltaic cells. *J Appl Phys* 101:114503-1–114503-12
45. Huynh WU, Dittmer JJ, Alivisatos AP (2002) Hybrid nanorod-polymer solar cells. *Science* 295:2425–2427
46. Kietzke T, Egbe DAM, Horhold HH, Neher D (2006) Comparative study of M3EH-PPV-based bilayer photovoltaic devices. *Macromolecules* 39:4018–4022
47. Koetse M, Sweelssen J, Hoekerd K, Schoo H (2006) Efficient polymer: polymer bulk heterojunction solar cells. *Appl Phys Lett* 88:083504-1–083504-3
48. McNeill CR, Abruci A, Zaumseil J, Wilson R, McKiernan MJ, Burroughes JH, Halls JMM, Greenham NC, Friend RH (2007) Dual electron donor/electron acceptor character of a conjugated polymer in efficient photovoltaic diodes. *Appl Phys Lett* 90:193506-1–193506-3
49. Ooi ZE, Tam TL, Shin RYC, Chen ZK, Kietzke T, Sellinger A, Baumgarten M, Mullen K, de Mello JC (2008) Solution processable bulk-heterojunction solar cells using a small molecule acceptor. *J Mater Chem* 18:4619–4622
50. Schubert M, Yin C, Castellani M, Bange S, Tam TL, Sellinger A, Hörhold H-H, Kietzke T, Neher D (2009) Heterojunction topology versus fill factor correlations in novel hybrid small-molecular/polymeric solar cells. *J Chem Phys* 130:094703-1–094703-9
51. Inal S, Castellani M, Sellinger A, Neher D (2009) Relationship of photophysical properties and the device performance of novel hybrid small-molecular/polymeric solar cells. *Macromol Rapid Commun* 30:1263–1268
52. Kietzke T, Shin RYC, Egbe DAM, Chen ZK, Sellinger A (2007) Effect of annealing on the characteristics of organic solar cells: polymer blends with a 2-vinyl-4, 5-dicyanoimidazole derivative. *Macromolecules* 40:4424–4428
53. Shin RYC, Kietzke T, Sudhakar S, Dodabalapur A, Chen Z-K, Sellinger A (2007) N-type conjugated materials based on 2-vinyl-4, 5-dicyanoimidazoles and their use in solar cells. *Chem Mater* 19:1892–1894
54. Martinson ABF, Massari AM, Lee SJ, Gurney RW, Splan KE, Hupp JT, Nguyen ST (2006) Organic photovoltaics interdigitated on the molecular scale. *J Electrochem Soc* 153:A527–A535
55. Smith ARG, Ruggles JL, Yu A, Gentle IR (2009) Multilayer nanostructured porphyrin arrays constructed by layer-by-layer self-assembly. *Langmuir* 25:9873–9878
56. Yui T, Kameyama T, Sasaki T, Torimoto T, Takagi K (2007) Pyrene-to-porphyrin excited singlet energy transfer in LBL-deposited LDH nanosheets. *J Porphyr Phthalocyanines* 11:428–433
57. Li LS, Jia QX, Li ADQ (2002) Effects of organic self-assembled polymer and metal phthalocyanine multilayers on the surface photovoltaic properties of indium tin oxide and titanium oxide. *Chem Mater* 14:1159–1165
58. Alencar WS, Crespihlo FN, Santos MRM, Zucolotto V, Oliveira ON Jr, Silva WC (2007) Influence of film architecture on the charge-transfer reactions of metallophthalocyanine layer-by-layer films. *J Phys Chem C* 111:12817–12821
59. Arakawa T, Munaoka T, Akiyama T, Yamada SW (2009) Effects of silver nanoparticles on photoelectrochemical responses of organic dyes. *J Phys Chem C* 113:11830–11835
60. Nishiyama F, Yokoyama T, Kamikado T, Yokoyama S, Mashiko S (2006) Layer-by-layer growth of porphyrin supramolecular thin films. *Appl Phys Lett* 88:253113-1–253113-3
61. Zhang B, Mu J, Li XQ (2006) Linear assemblies of aged CdS particles and cationic porphyrin in multilayer films. *Appl Surf Sci* 252:4990–4994
62. Alencar WS, Crespihlo FN, Martins MVA, Zucolotto V, Oliveira ON, Silva WC (2009) Synergistic interaction between gold nanoparticles and nickel phthalocyanine in layer-by-layer (LbL) films: evidence of constitutional dynamic chemistry (CDC). *Phys Chem Chem Phys* 11:5086–5091

63. Pradhan B, Bandyopadhyay A, Pal AJ (2004) Molecular level control of donor/acceptor heterostructures in organic photovoltaic devices. *Appl Phys Lett* 85:663–665
64. Bente H, Kudo N, Ohkita H, Ito S (2009) Layer-by-layer deposition films of copper phthalocyanine derivative; their photoelectrochemical properties and application to solution-processed thin-film organic solar cells. *Thin Solid Films* 517:2016–2022
65. Forrest SR (1997) Ultrathin organic films grown by organic molecular beam deposition and related techniques. *Chem Rev* 97:1793–1896
66. Shtein M, Gossenberger HF, Benziger JB, Forrest SR (2001) Material transport regimes and mechanisms for growth of molecular organic thin films using low-pressure organic vapor phase deposition. *J Appl Phys* 89:1470–1476
67. Ling MM, Bao ZN (2004) Thin film deposition, patterning, and printing in organic thin film transistors. *Chem Mater* 16:4824–4840
68. Burrows PE, Forrest SR, Buma T, Fenter P, Sapochak LS, Schwartz J, Ban VS, Forrest JL (1995) Organic vapor phase deposition: a new method for the growth of organic thin films with large optical non-linearities. *J Cryst Growth* 156:91–98
69. Baldo M, Deutsch M, Burrows P, Gossenberger H, Gerstenberg M, Ban V, Forrest SR (1998) Organic vapor phase deposition. *Adv Mater* 10:1505–1514
70. Shtein M, Peumans P, Benziger JB, Forrest SR (2003) Micropatterning of small molecular weight organic semiconductor thin films using organic vapor phase deposition. *J Appl Phys* 93:4005–4016
71. Shtein M, Mapel J, Benziger JB, Forrest SR (2002) Effects of film morphology and gate dielectric surface preparation on the electrical characteristics of organic-vapor-phase-deposited pentacene thin-film transistors. *Appl Phys Lett* 81:268–270
72. Rand BP, Genoe J, Heremans P, Poortmans J (2007) Solar cells utilizing small molecular weight organic semiconductors. *Prog Photovoltaics* 15:659–676
73. Meiss J, Leo K, Riede MK, Uhrich C, Gnehr W-M, Sonntag S, Pfeiffer M (2009) Efficient semitransparent small-molecule organic solar cells. *Appl Phys Lett* 95:213306
74. Rusu M, Wiesner S, Mete T, Blei H, Meyer N, Heuken M, Lux-Steiner MC, Fostiropoulos K (2008) Organic donor, acceptor and buffer layers of small molecules prepared by OVPD technique for photovoltaics. *Renew Energy* 33:254–258
75. Peumans P, Bulovic V, Forrest SR (2000) Efficient photon harvesting at high optical intensities in ultrathin organic double-heterostructure photovoltaic diodes. *Appl Phys Lett* 76:2650–2652
76. Vogel M, Doka S, Breyer C, Lux-Steiner MC, Fostiropoulos K (2006) On the function of a bathocuproine buffer layer in organic photovoltaic cells. *Appl Phys Lett* 89:163501
77. Breyer C, Vogel M, Mohr M, Johnev B, Fostiropoulos K (2006) Influence of exciton distribution on external quantum efficiency in bilayer organic solar cells. *Physica Status Solidi (b)* 243:3176–3180
78. Peumans P, Uchida S, Forrest SR (2003) Efficient bulk heterojunction photovoltaic cells using small-molecular weight organic thin films. *Nature* 425:158–162
79. Dittmer JJ, Lazzaroni R, Leclère P, Moretti P, Granström M, Petritsch K, Marseglia EA, Friend RH, Brédas JL, Rost H, Holmes AB (2000) Crystal network formation in organic solar cells. *Sol Energy Mater Sol Cells* 61:53–61
80. Gebeyehu D, Maennig B, Drechsel J, Leo K, Pfeiffer M (2003) Bulk-heterojunction photovoltaic devices based on donor–acceptor organic small molecule blends. *Sol Energy Mater Sol Cells* 79:81–92
81. Pannemann C, Dyakonov V, Parisi J, Hild O, Wöhrle D (2001) Electrical characterization of zinc-phthalocyanine-fullerene photovoltaic cells. *Synth Metals* 121:1585
82. Geens W, Aernouts T, Poortmans J, Hadziioannou G (2002) Organic co-evaporated films of a PPV-pentamer and C-60: model systems for donor/acceptor polymer blends. *Thin Solid Films* 403:438–443
83. Günes S, Neugebauer H, Sariciftci NS (2007) Conjugated polymer-based organic solar cells. *Chem Rev* 107:1324–1338

84. Granström M, Pertritsch K, Arias AC, Lux A, Andersson MR, Friend RH (1998) Laminated fabrication of polymeric photovoltaic diodes. *Nature* 395:257–260
85. Yu G, Gao J, Hummelen JC, Wudl F, Heeger AJ (1995) Polymer photovoltaic cells: enhanced efficiencies via a network of internal donor–acceptor heterojunctions. *Science* 270:1789–1791
86. Hiramoto M, Yamaga T, Danno M, Suemori K, Matsumura Y, Yokoyama M (2006) Design of nanostructures for photoelectric conversion using an organic vertical superlattice. *Appl Phys Lett* 88:213105
87. Liang Y, Xu Z, Xia J, Tsai ST, Wu Y, Li G, Ray C, Yu L (2010) For the bright future—bulk heterojunction polymer solar cells with power conversion efficiency of 7.4%. *Adv Mater* 22:1–4
88. Feng W, Fujii A, Lee S, Wu H, Yoshino K (2000) Broad spectral sensitization of organic photovoltaic heterojunction device by perylene and C60. *J Appl Phys* 88:7120–7123
89. Tsuzuki T, Shirota Y, Rostalski J, Meissner D (2000) The effect of fullerene doping on photoelectric conversion using titanyl phthalocyanine and a perylene pigment. *Sol Energy Mater Sol Cells* 61:1–8
90. Hiramoto M, Suemori K, Yokoyama M (2002) Photovoltaic properties of ultramicrostructure controlled organic co-deposited films. *Jpn J Appl Phys* 41:2763–2766
91. Halls JJM, Friend RH (1997) The photovoltaic effect in a poly(p-phenylenevinylene)/perylene heterojunction. *Synth Metals* 85:1307–1308
92. Rand BP, Xue J, Uchida S, Forrest SR (2005) Mixed donor acceptor molecular heterojunctions for photovoltaic applications. I. Material properties. *J Appl Phys* 98:124902
93. Uchida S, Xue J, Rand BP, Forrest SR (2004) Organic small molecule solar cells with a homogeneously mixed copper phthalocyanine: C60 active layer. *Appl Phys Lett* 84:4218–4220
94. Heutz S, Sullivan P, Sanderson BM, Schultes SM, Jones TS (2004) Influence of molecular architecture and intermixing on the photovoltaic, morphological and spectroscopic properties of CuPc-C60 heterojunctions. *Sol Energy Mater Sol Cells* 83:229–245
95. Sullivan P, Heutz S, Schultes SM, Jones TS (2004) Influence of codeposition on the performance of CuPc-C-60 heterojunction photovoltaic devices. *Appl Phys Lett* 84:1210–1212
96. Xue J, Rand BP, Uchida S, Forrest SR (2005) Mixed donor acceptor molecular heterojunctions for photovoltaic applications. II. Device performance. *J Appl Phys* 98:124903
97. Opitz A, Bronner M, Bruetting W (2007) Ambipolar charge carrier transport in mixed organic layers of phthalocyanine and fullerene. *J Appl Phys* 101:063709
98. Mihailetchi VD, Koster LJA, Blom PWM, Melzer C, de Boer B (2005) Compositional dependence of the performance of poly(p-phenylene vinylene): methanofullerene bulk-heterojunction solar cells. *Adv Funct Mater* 15:795–801
99. Yang F, Shtein M, Forrest SR (2005) Controlled growth of a molecular bulk heterojunction photovoltaic cell. *Nat Mater* 4:37–41
100. Xue J, Uchida S, Rand BP, Forrest SR (2004) 4.2% efficient organic photovoltaic cells with low series resistances. *Appl Phys Lett* 84:3013–3015
101. Xue J, Rand BP, Uchida S, Forrest SR (2005) A hybrid planar-mixed molecular heterojunction photovoltaic cell. *Adv Mater* 17:66–70
102. Shockley W, Queisser HJ (1961) Detailed balance limit of efficiency of p–n junction solar cells. *J Appl Phys* 32:510
103. Schueppel R, Timmreck R, Allinger N, Mueller T, Furno M, Uhrich C, Leo K, Riede M (2010) Controlled current matching in small molecule organic tandem solar cells using doped spacer layers. *J Appl Phys* 107:044503
104. Hadipour A, De Boer B, Blom PWM (2008) Organic tandem and multi-junction solar cells. *Adv Funct Mater* 18:169–181
105. Hadipour A, De Boer B, Blom PMW (2008) Device operation of organic tandem solar cells. *Org Electron* 9:617–624

106. Ameri T, Dennler G, Lungenschmied C, Brabec CJ (2009) Organic tandem solar cells: a review. *Energy Environ Sci* 2:347–363
107. Hiramoto M, Suezaki M, Yokoyama M (1990) Effect of thin gold interstitial-layer on the photovoltaic properties of tandem organic solar cell. *Chem Lett* 19:327–330
108. Forrest SR (2005) The limits to organic photovoltaic cell efficiency. *MRS Bull* 30:28–32
109. Yakimov A, Forrest SR (2002) High photovoltage multiple-heterojunction organic solar cells incorporating interfacial metallic nanoclusters. *Appl Phys Lett* 80:1667–1669
110. Rand BP, Peumans P, Forrest SR (2004) Long-range absorption enhancement in organic tandem thin-film solar cells containing silver nanoclusters. *J Appl Phys* 12:7519–7526
111. Triyana K, Yasuda T, Fujita K, Tsutsui T (2004) Effects of different materials used for internal floating electrode on the photovoltaic properties of tandem type organic solar cell. *Jpn J Appl Phys Part I* 43:2352–2356
112. Triyana K, Yasuda T, Fujita K, Tsutsui T (2004) Organic tandem and multi junction solar cells. *Thin Solid Films* 447:198–202
113. Xue J, Uchida S, Rand BP, Forrest SR (2004) Asymmetric tandem organic photovoltaic cells with hybrid planar-mixed molecular heterojunctions. *Appl Phys Lett* 85:5757–5759
114. Peumans P, Yakimov A, Forrest SR (2003) Small molecular weight organic thin-film photodetectors and solar cells. *J Appl Phys* 93:3693–3723
115. Drechsel J, Männig B, Kozłowski F, Pfeiffer M, Leo K (2005) Efficient organic solar cells based on a double p–i–n architecture using doped wide-gap transport layers. *Appl Phys Lett* 86:244102
116. Yu B, Zhu F, Wang H, Li G, Yan D (2008) All-organic tunnel junctions as connecting units in tandem organic solar cell. *J Appl Phys* 104:114503
117. Chandrasekhar S, Sadashiva BK, Suresh KA (1977) Liquid-crystals of disc-like molecules. *Pramana* 9:471–480
118. Kumar S (2006) Self-organization of disc-like molecules: chemical aspects. *Chem Soc Rev* 35:83–109
119. Adam D, Schuhmacher P, Simmerer J, Haussling L, Siemensmeyer K, Etbacj KH, Ringsdorf H, Haarer D (1994) Fast photoconduction in the highly ordered columnar phase of a discotic liquid-crystal. *Nature* 371:141–143
120. van de Craats AM, Warman JM, Fechtenkötter A, Brand JD, Harbison MA, Müllen K (1999) Record charge carrier mobility in a room-temperature discotic liquid-crystalline derivative of hexabenzocoronene. *Adv Mater* 11:1469–1472
121. Sergeev S, Pisula W, Geerts Y (2007) Discotic liquid crystals: a new generation of organic semiconductors. *Chem Soc Rev* 36:1902–1929
122. Woon KL, Aldred MP, Richards GJ, Vlachos P, Mehl GH, Kelly SM, O'Neill M (2006) Electronic charge transport in extended nematic liquid crystals. *Chem Mater* 18:2311–2317
123. Kumar S (2002) Discotic liquid crystals for solar cells. *Curr Sci India* 82:256–257
124. Grelet E, Bock H (2006) Control of the orientation of thin open supported columnar liquid crystal films by the kinetics of growth. *Europhys Lett* 73:712–718
125. Archambeau S, Seguy I, Jolinat P, Farenc J, Destruel P, Nguyen TP, Bock H, Grelet E (2006) Stabilization of discotic liquid organic thin films by ITO surface treatment. *Appl Surf Sci* 253:2078–2086
126. Charlet E, Grelet E, Brettes P, Bock H, Saadaoui H, Cisse I, Destruel P, Gherardi N, Seguy I (2008) Ultrathin films of homeotropically aligned columnar liquid crystals on indium tin oxide electrodes. *Appl Phys Lett* 92:024107-1–024107-3
127. Schmidt-Mende L, Fechtenkötter A, Müllen K, Moons E, Friend RH, MacKenzie JD (2001) Self-organized discotic liquid crystals for high-efficiency organic photovoltaics. *Science* 293:1119–1122
128. Lemaire V, Da Silva Filho DA, Coropceanu V, Lehmann M, Greets Y, Piris J, Debije MG, van de Craats AM, Senthilkumar K, Siebbeles LDA, Warman JM, Bredas JL, Cornil J (2004) Charge transport properties in discotic liquid crystals: a quantum-chemical insight into structure–property relationships. *J Am Chem Soc* 126:3271–3279

129. van de Craats AM, Warman JM (2001) The core-size effect on the mobility of charge in discotic liquid crystalline materials. *Adv Mater* 13:130–133
130. Tracz A, Jeszka JK, Watson MD, Pisula W, Müllen K, Pakula T (2003) Uniaxial alignment of the columnar super-structure of a hexa (alkyl) hexa-peri-hexabenzocoronene on untreated glass by simple solution processing. *J Am Chem Soc* 125:1682–1683
131. Pisula W, Tomovi Z, El Hamaoui B, Watson MD, Pakula T, Müllen K (2005) Control of the homeotropic order of discotic hexa-peri-hexabenzocoronenes. *Adv Funct Mater* 15:893–904
132. Li J, Kastler M, Pisula W, Willem J, Robertson F, Wasserfallen D, Grimsdale AC, Wu J, Müllen K (2007) Organic bulk-heterojunction photovoltaics based on alkyl substituted discotics. *Adv Funct Mater* 17:2528–2533
133. Wong WWH, Ma C-Q, Pisula W, Yan C, Feng X, Jones DJ, Müllen K, Janssen RA, Bäuerle P, Holmes AB (2010) Self-assembling thiophene dendrimers with a hexa-peri-hexabenzocoronene core-synthesis, characterization and performance in bulk heterojunction solar cells. *Chem Mater* 22:457–466
134. Schmidt-Mende L, Fechtenkötter A, Müllen K, Friend RH, MacKenzie JD (2002) Efficient organic photovoltaics from soluble discotic liquid crystalline materials. *Physica E* 14:263–267
135. Liu S-G, Sui G, Cormier RA et al (2002) Self-organizing liquid crystal perylene diimide thin films: spectroscopy, crystallinity, and molecular orientation. *J Phys Chem B* 106:1307–1315
136. Schmidt-Mende L, Watson M, Müllen K, Friend RH (2003) Organic thin film photovoltaic devices from discotic materials. *Mol Cryst Liq Cryst* 396:73–90
137. Schmidtke JP, Friend RH, Kastler M, Müllen K (2006) Control of morphology in efficient photovoltaic diodes from discotic liquid crystals. *J Chem Phys* 124:175704-1–175704-6
138. Gregg BA, Fox MA, Bard AJ (1990) Photovoltaic effect in symmetrical cells of a liquid-crystal porphyrin. *J Phys Chem* 94:1586–1598
139. Petristich K, Friend RH, Lux A, Rozenberg G, Moratti SC, Holmes AB (1999) Liquid crystalline phthalocyanines in organic solar cells. *Synth Metals* 102:1776–1777
140. Levitsky IA, Euler WB, Tokranova N, Xu B, Castracane J (2004) Hybrid solar cells based on porous Si and copper phthalocyanine derivatives. *Appl Phys Lett* 85:6245–6247
141. Boden N, Bushby RJ, Clements J (1993) Mechanism of quasi-one-dimensional electronic conductivity in discotic liquid-crystals. *J Chem Phys* 98:5920–5931
142. Boden N, Bushby RJ, Cammidge AN, Clements J, Luo R, Donovan KJ (1995) Transient photoconductivity and dark conductivity in discotic liquid crystals. *Mol Cryst Liq Cryst* 261:251–257
143. Kumar S, Pal SK, Kumar PS, Lakshminarayanan V (2007) Novel conducting nanocomposites: synthesis of triphenylene-covered gold nanoparticles and their insertion into a columnar matrix. *Soft Matter* 3:896–900
144. Kumar PS, Kumar S, Lakshminarayanan V (2008) Electrical conductivity studies on discotic liquid crystal-ferrocenium donor–acceptor systems. *J Phys Chem B* 112:4865–4869
145. Kumar PS, Kumar S, Lakshminarayanan V (2009) Hybrid organic/inorganic nanocomposite as a quasi-one-dimensional semiconductor under ambient conditions. *J Appl Phys* 106:093701-1–093701-6
146. Schmidt J, Dierking I (2001) Localization and imaging of local shunts in solar cells using polymer-dispersed liquid crystals. *Prog Photovoltaics* 9:263–271
147. Koeppel R, Bossart O, Calzaferre G, Sariciftci NS (2007) Advanced photon-harvesting concepts for low-energy gap organic solar cells. *Sol Energy Mater Sol Cells* 91:986–995
148. Liu YX, Summers MA, Edder C, Frechet JMJ, McGehee MD (2005) Using resonance energy transfer to improve exciton harvesting in organic–inorganic hybrid photovoltaic cells. *Adv Mater* 17:2960–2964
149. Hong ZR, Lessmann R, Maennig B, Huang Q, Harada K, Riede M, Leo K (2009) Antenna effects and improved efficiency in multiple heterojunction photovoltaic cells based on pentacene, zinc phthalocyanine, and C60. *J Appl Phys* 106:064511-1–064511-6
150. Imahori H, Fukuzumi S (2004) Porphyrin- and fullerene-based molecular photovoltaic devices. *Adv Funct Mater* 14:525–536

151. Zhang C, Tong SW, Jiang C, Kang ET, Chan DSH, Zhu CX (2008) Efficient multi-layer organic solar cells using the optical interference peak. *Appl Phys Lett* 93:043307-1–043307-3
152. Dastoor PC, McNeill CR, Frohne H, Foster CJ, Dean B, Fell CJ, Belcher WJ, Campbell WM, Officer DL, Blake IM, Thordarson P, Crossley MJ, Hush NS, Reimers JR (2007) Understanding and improving solid-state polymer/C60-fullerene bulk-heterojunction solar cells using ternary porphyrin blends. *J Phys Chem C* 111:15415–15426
153. Burke KB, Belcher WJ, Thomsen L, Watts B, McNeill CR, Ade H, Dastoor PC (2009) Role of solvent trapping effects in determining the structure and morphology of ternary blend organic devices. *Macromolecules* 42:3098–3103
154. Belcher WJ, Wagner KI, Dastoor PC (2007) The effect of porphyrin inclusion on the spectral response of ternary P3HT:porphyrin:PCBM bulk heterojunction solar cells. *Sol Energy Mater Sol Cells* 91:447–452
155. Shao Y, Yang Y (2005) Efficient organic heterojunction photovoltaic cells based on triplet materials. *Adv Mater* 17:2841–2844
156. Schulz GL, Holdcroft S (2008) Conjugated polymers bearing iridium complexes for triplet photovoltaic devices. *Chem Mater* 20:5351–5355
157. Yang C-M, Wu C-H, Liao H-H, Lai KY, Cheng HP, Horng SF, Meng HF, Shy JT (2007) Enhanced photovoltaic response of solar cell by singlet-to-triplet exciton conversion. *Appl Phys Lett* 90:133509-1–133509-3
158. Li Y, Mastria R, Li K, Fiore A, Wang Y, Cingolani R, Manna L, Gigli G (2009) Improved photovoltaic performance of bilayer heterojunction photovoltaic cells by triplet materials and tetrapod-shaped colloidal nanocrystals doping. *Appl Phys Lett* 95:043101-1–043101-3
159. Guo FQ, Kim YG, Reynolds JR, Schanze KS (2006) Platinum-acetylide polymer based solar cells: involvement of the triplet state for energy conversion. *Chem Commun* 1887–1889
160. Hatton RA, Blanchard NP, Miller AJ, Silva SRP (2007) A multi-wall carbon nanotube-molecular semiconductor composite for bi-layer organic solar cells. *Physica E* 37:124–127
161. Hatton RA, Blanchard NP, Stolojan V, Miller AJ, Silva SRP (2007) Nanostructured copper phthalocyanine-sensitized multiwall carbon nanotube films. *Langmuir* 23:6424–6430
162. O'Regan B, Grätzel M (1991) A low-cost, high-efficiency solar cell based on dye-sensitized colloidal TiO₂ films. *Nature* 353:737–740
163. Grätzel M (2001) Measured under standard air mass 1.5 reporting conditions, PV calibration. Laboratory of the National Energy Research Laboratory (NREL), Golden
164. Hinsch A, Kroon JM, Späth M, van Roosmale JAM, Bakker NJ, Sommeling P, van der Burg N, Kinderman R, Kern R, Ferber J, Schill C, Schubert M, Meyer A, Meyer T, Uhlendorf I, Holzbock J, Niepmann R (2000) In: Proceedings of the 16th European photovoltaic solar energy conference and exhibition, Glasgow
165. Nogueira AF, Durrant JR, De Paoli M-A (2001) Dye-sensitized nanocrystalline solar cells employing a polymer electrolyte. *Adv Mater* 13:826–830
166. De Freitas JN, Nogueira AF, De Paoli M-A (2009) New insights into dye-sensitized solar cells with polymer electrolytes. *J Mater Chem* 19:5279–5294
167. Freitas FS, De Freitas JN, Ito BI, De Paoli M-A, Nogueira AF (2009) Electrochemical and structural characterization of polymer gel electrolytes based on a PEO copolymer and an imidazolium-based ionic liquid for dye-sensitized solar cells. *Appl Mater Interfaces* 1:2870–2877
168. Bach U, Lupo D, Comte P, Moser JE, Weissortel F, Salbeck J, Spreitzer H, Grätzel M (1998) Solid-state dye-sensitized mesoporous TiO₂ solar cells with high photon-to-electron conversion efficiencies. *Nature* 395:583–585
169. Kroeze JE, Hirata N, Schmidt-Mende L, Orizu C, Ogier SD, Carr K, Grätzel M, Durrant JR (2006) Parameters influencing charge separation in solid-state dye-sensitized solar cells using novel hole conductors. *Adv Func Mater* 16:1832–1838
170. Poplavskyy D, Nelson J (2003) Nondispersive hole transport in amorphous films of methoxy-spirofluorene-arylamine organic compound. *J Appl Phys* 93:341–346

171. Zhao Y, Chen W, Zhai J, Sheng X, He Q, Wei T, Bai F, Jiang L, Zhu D (2007) Solid-state dye-sensitized photovoltaic device with newly designed small organic molecule as hole-conductor. *Chem Phys Lett* 445:259–264
172. Hagena J, Schaffrath W, Otschik P, Fink R, Bacher A, Schmidt H-W, Haarer D (1997) Novel hybrid solar cells consisting of inorganic nanoparticles and an organic hole transport material. *Synth Metals* 89:215–220
173. Karthikeyan CS, Thelakkat M (2008) Key aspects of individual layers in solid-state dye-sensitized solar cells and novel concepts to improve their performance. *Inorg Chim Acta* 361:635–655
174. Tian H, Meng F (2005) Solar cells based on cyanine and polymethine dyes. In: Sun S-S, Sariciftci NS (eds) *Organic photovoltaics*, 1st edn. Taylor & Francis, Boca Raton
175. Horiuchi T, Miura H, Sumioka K, Uchida S (2004) High efficiency of dye-sensitized solar cells based on metal-free indoline dyes. *J Am Chem Soc* 126:12218–12219
176. Ito S, Miura H, Uchida S, Takata M, Sumioka K, Liska P, Comte P, Péchy P, Grätzel M (2008) High-conversion-efficiency organic dye-sensitized solar cells with a novel indoline dye. *Chem Commun* 5194–5196
177. O'Regan B, Lenzmann F (2004) Charge transport and recombination in a nanoscale interpenetrating network of n-type and p-type semiconductors: transient photocurrent and photovoltage studies of TiO₂/Dye/CuSCN photovoltaic cells. *J Phys Chem B* 108:4342–4350
178. Snaith HJ, Moule AJ, Klein C, Meerholz K, Friend RH, Grätzel M (2007) Efficiency enhancements in solid-state hybrid solar cells via reduced charge recombination and increased light capture. *Nano Lett* 7:3372–3376
179. Schmidt-Mende L, Grätzel M (2006) TiO₂ pore-filling and its effect on the efficiency of solid-state dye-sensitized solar cells. *Thin Solid Films* 500:296–301
180. Boschloo GK, Goossens A (1996) Electron trapping in porphyrin-sensitized porous nanocrystalline TiO₂ electrodes. *J Phys Chem* 100:19489–19494
181. Wienke J, Schaafsma TJ, Goossens A (1999) Visible light sensitization of titanium dioxide with self-organized porphyrins: organic P–I–N solar cells. *J Phys Chem B* 103:2702–2708
182. Savenije TJ, Goossens A (2001) Hole transport in porphyrin thin films. *Phys Rev B* 64:115323
183. Miyairi K, Itoh E, Hashimoto Y (2003) Photovoltaic properties of double layer devices consisting of titanium dioxide and porphyrin dispersed hole transporting material layer. *Thin Solid Films* 438–439:147–152
184. Simon J, Andre JJ (1998) *Molecular semiconductors, photoelectrical properties and solar cells*. Springer, Berlin
185. Gregg BA (1996) Bilayer molecular solar cells on spin-coated TiO₂ substrates. *Chem Phys Lett* 258:376–380
186. Signerski R, Jarosz G, Koscielska B (2009) On photovoltaic effect in hybrid heterojunction formed from palladium phthalocyanine and titanium dioxide layers. *J Non-Crystalline Solids* 355:1405–1407
187. Sharma GD, Kumar R, Roy MS (2006) Investigation of charge transport, photo generated electron transfer and photovoltaic response of iron phthalocyanine (FePc):TiO₂ thin films. *Sol Energy Mater Sol Cells* 90:32–45
188. Tracey SM, Hodgson SNB, Ray AK (1998) Sol–gel derived TiO₂/lead phthalocyanine photovoltaic cells. *J. Sol–Gel Sci. Techn* 13:219–222
189. Kajihara K, Tanaka K, Hirao K, Soga N (1996) Photovoltaic effect in titanium dioxide/zinc phthalocyanine cell. *Jpn J Appl Phys* 35:6110–6116
190. Ohmori Y, Itoh E, Miyairi K (2006) Photovoltaic properties of phthalocyanine based p–n diode evaporated onto titanium dioxide. *Thin Solid Films* 499:369–373
191. Tachibana Y, Haque SA, Mercer IP, Durrant JR, Klug DR (2000) Electron injection and recombination in dye sensitized nanocrystalline titanium dioxide films: a comparison of ruthenium bipyridyl and porphyrin sensitizer dyes. *J Phys Chem B* 104:1198–1205

192. Imahori H, Umeyama T, Ito S (2009) Large-aromatic molecules as potential sensitizers for highly efficient dye-sensitized solar cells. *Acc Chem Res* 42:1809–1818
193. Campbell WM, Burrell AK, Officer DL, Jolley KW (2004) Porphyrins as light harvesters in the dye-sensitized TiO₂ solar cell. *Coord Chem Rev* 248:1363–1379
194. Lee CY, Hupp JT (2010) Dye sensitized solar cells: TiO₂ sensitization with a bodipy-porphyrin antenna system. *Langmuir* 26:3760–3765
195. Nazeeruddin MK, Humphry-Baker R, Grätzel M, Murrer BA (1998) Efficient near IR sensitization of nanocrystalline TiO₂ films by ruthenium phthalocyanine. *Chem Commun* 719–720
196. Yum J-H, Jang S-R, Humphry-Baker R, Grätzel M, Cid J-J, Torres T, Nazeeruddin MK (2008) Effect of coadsorbent on the photovoltaic performance of zinc phthalocyanine-sensitized solar cells. *Langmuir* 24:5636–5640
197. Shen L, Zhu G, Guo W, Tao C, Zhang X, Liu C, Chen W, Ruan S, Zhong Z (2008) Performance improvement of TiO₂/P3HT solar cells using CuPc as a sensitizer. *Appl Phys Lett* 92:073307
198. Morandeira A, López-Duarte I, O'Regan B, Martínez-Díaz MV, Forneli A, Palomares E, Torres T, Durrant JR (2009) Ru(II)-phthalocyanine sensitized solar cells: the influence of co-adsorbents upon interfacial electron transfer kinetics. *J Mater Chem* 19:5016–5026
199. Schouten PG, Warman JM, De haas MP, Fox MA, Pan HL (1991) Charge migration in supramolecular stacks of peripherally substituted porphyrins. *Nature* 353:736–737
200. Lawrence MF, Huang Z, Langford CH, Ordonez I (1993) Photocurrent generation and charge transport in tin dioxide/ion-exchange polymer-zinc meso-tetraphenylporphyrin/gold cells. *J Phys Chem* 97:944–951
201. Taleb T, Nasr C, Hotchandani S, Leblanc RM (1996) Effect of temperature on capacitance of Al/microcrystalline chlorophylla/Ag sandwich cells. *J Appl Phys* 79:1701
202. Ioannidis A, Lawrence MF, Kassi H, Cote R, Dodelet JP, Leblanc RM (1993) Field dependence of hole mobilities in chloro-aluminum phthalocyanine. *Chem Phys Lett* 205:46–50
203. Senadeera GKR, Jayaweera PVV, Perera VPS, Tennakone K (2002) Solid-state dye-sensitized photocell based on pentacene as a hole collector. *Sol Energy Mater Sol Cells* 73:103–108
204. Zhang G, Bala H, Cheng Y, Shi D, Lv X, Yu Q, Wang P (2009) High efficiency and stable dye-sensitized solar cells with an organic chromophore featuring a binary π -conjugated spacer. *Chem Commun* 2198–2200
205. Hara K, Tachibana Y, Ohga Y, Shinpo A, Suga S, Sayama K, Sugihara H, Arakawa H (2003) Dye-sensitized nanocrystalline TiO₂ solar cells based on novel coumarin dyes. *Sol Energy Mater Sol Cells* 77:89–103
206. Zafer C, Kus M, Turkmen G, Dincalp H, Demic S, Kuban B, Teoman Y, Icli S (2007) New perylene derivative dyes for dye-sensitized solar cells. *Sol Energy Mater Sol Cells* 91:427–431
207. Shibano Y, Umeyama T, Matano Y, Imahori H (2007) Electron-donating perylene tetracarboxylic acids for dye-sensitized solar cells. *Org Lett* 9:1971–1974
208. Fortage J, Séverac M, Houarner-Rassin C, Pellegrin Y, Blart E, Odobel F (2008) Synthesis of new perylene imide dyes and their photovoltaic performances in nanocrystalline TiO₂ dye-sensitized solar cells. *J Photochem Photobiol A Chem* 197:156–169
209. Jin Y, Hua J, Wu W, Ma X, Meng F (2008) Synthesis, characterization and photovoltaic properties of two novel near-infrared absorbing perylene dyes containing benzo[e]indole for dye-sensitized solar cells. *Synth Metals* 158:64–71
210. Zhang G, Bai Y, Li R, Shi D, Wenger S, Zakeeruddin SM, Grätzel M, Wang P (2009) Employ a bithienothiophene linker to construct an organic chromophore for efficient and stable dye-sensitized solar cells. *Energy Environ Sci* 2:92–95
211. Xu M, Li R, Pootrakulchote N, Shi S, Guo J, Yi Z, Zakeeruddin SM, Grätzel M, Wang P (2008) Energy-level and molecular engineering of organic D- π -A sensitizers in dye-sensitized solar cells. *J Phys Chem C* 112:19770–19776

212. Schmidt-Mende L, Bach U, Humphry-Baker R, Horiuchi T, Miura H, Ito S, Uchida S, Grätzel M (2005) Organic dye for highly efficient solid-state dye-sensitized solar cells. *Adv Mater* 17:813–815
213. Kuang D, Uchida S, Humphry-Baker R, Zakeeruddin SM, Grätzel M (2008) Organic dye-sensitized ionic liquid based solar cells: remarkable enhancement in performance through molecular design of indoline sensitizers. *Angew Chem Int Ed* 47:1923–1927
214. Grätzel M (2009) Recent advances in sensitized mesoscopic solar cells. *Acc Chem Res* 42(11):1788–1798
215. Yum J-H, Hagberg DP, Moon S-J, Karlsson KM, Marinado T, Sun L, Hagfeldt A, Nazeeruddin MK, Grätzel M (2009) A light-resistant organic sensitizer for solar-cell applications. *Angew Chem Int Ed* 48:1576–1580
216. Choi H, Baik C, Kang SO, Ko J-J, Kang M-S, Nazeeruddin MK, Grätzel M (2008) Highly efficient and thermally stable organic sensitizers for solvent-free dye-sensitized solar cells. *Angew Chem Int Ed* 47:327–330
217. Haque SA, Park T, Holmes AB, Durrant JR (2003) Transient optical studies of interfacial energetic disorder at nanostructured dye-sensitized inorganic/organic semiconductor heterojunctions. *ChemPhysChem* 4:89–93
218. O'Regan B, Schwartz DT (1998) Large enhancement in photocurrent efficiency caused by UV illumination of the dye-sensitized heterojunction TiO₂/RuLL'NCS/CuSCN: initiation and potential mechanisms. *Chem Mater* 10:1501–1509
219. Tennakone K, Kumara G, Kumarasinghe AR, Wijayantha KGU, Sirimanne PM (1995) A dye-sensitized nano-porous solid-state photovoltaic cell. *Semicond Sci Technol* 10:1689–1693
220. Tennakone K, Senadeera GKR, De Silva D, Kottegoda IRM (2000) Highly stable dye-sensitized solid-state solar cell with the semiconductor 4CuBr 3S(C₄H₉)₂ as the hole collector. *Appl Phys Lett* 77:2367